universität wien

# DIPLOMARBEIT

Titel der Diplomarbeit

AMS detection of $^{10}$Be
with a SiN-foil stack

Verfasser

Edith Schmidt, Bakk. rer. nat.

angestrebter akademischer Grad

Magistra der Naturwissenschaften (Mag. rer. nat.)

Wien, 2013

| | |
|---|---|
| Studienkennzahl lt. Studienblatt: | A-411 |
| Studienrichtung lt. Studienblatt: | Diplomstudium Physik |
| Betreuer: | Univ.-Prof. Dipl.-Ing. Dr. Robin Golser |

Ich widme meine Diplomarbeit meiner Mutter, die vor wenigen Jahren einer kurzen, schweren Krankheit erlag und deshalb den Abschluss meines Studiums nicht mehr erleben durfte.

# Abstract

$^{10}$Be (beryllium), with a half-life of (1.387 ± 0.012) Ma, is a long-lived, naturally occurring radioisotope. It is a cosmogenic nuclide, produced in the atmosphere and in-situ in surface rocks. $^{10}$Be therefore carries valuable signals for climate research and also is the primary tool for exposure dating in geology. Accelerator Mass Spectrometry (AMS) with its outstanding abundance sensitivity is the only technique capable of detecting $^{10}$Be at natural levels. Here, the challenge is to separate it form its stable isobar $^{10}$B. Based on almost perfectly homogeneous silicon nitride foils (SiN), a new AMS-method has been developed to detect $^{10}$Be at the Vienna Environmental Research Accelerator (VERA).
The dependence of energy-loss in matter from the atomic number is used to induce a difference in kinetic energy between $^{10}$Be and its stable isobar $^{10}$B before they are detected in an ionization chamber. To find the optimal setup, detailed simulations were performed. Until now, two other methods are used which are available at VERA and are commonly used at other facilities: absorption of $^{10}$B in a gas cell, and the use of a degrader foil followed by a magnetic separator. For comparison, environmental samples have been remeasured and compared to the results of the new foil stack method.

With the new foil stack method, that was developed during this thesis, the advantages of both methods have been combined. The significantly higher detection efficiency of 45 % provides superior precision with a reproducibility better than 0.3 %. The background has been reduced to $^{10}\mathrm{Be}/^{9}\mathrm{Be} = 7 \times 10^{-16}$, which makes the measurement of very low values possible. The foil stack method will replace the old method at VERA for future measurements.

# Zusammenfassung

$^{10}$Be (Beryllium) ist ein natürlich vorkommendes Radionuklid mit einer Halbwertszeit von $(1.387 \pm 0.012)$ Ma. Es entsteht in der Atmosphäre und in Gesteinsoberflächen durch den Einfluss der kosmischen Strahlung und ist daher ein nützlicher Tracer in der Klimaforschung und für geologische Anwendungen.
Die Messung dieser natürlichen, sehr geringen $^{10}$Be Häufigkeit und die Unterscheidung vom wesentlich häufigeren, stabilen $^{10}$B (Bor) ist selbst mittels AMS (Accelerator Mass Spectrometry) mit seiner hervorragenden Sensitivität eine Herausforderung.
Mit Hilfe von sehr homogenen Silizium Nitrid-Folien wurde bei VERA (Vienna Environmental Research Accelerator) eine neue Messmethode entwickelt. Durch den unterschiedlichen Energieverlust in Materie von Ionen verschiedener Kernladung wird der überwiegende Teil des $^{10}$B bereits in den Folien gestoppt. Die $^{10}$Be Ionen erreichen die dahinter liegende Ionisationskammer, wo sie von den restlichen Bor- und anderen Hintergrund-Ionen unterschieden werden können. Ausführliche Simulationen zum Energieverlust in SRIM trugen dazu bei, das optimale Setup zu finden.
Zusätzlich wurden teilweise bereits bekannte Proben erneut gemessen, um die neue Messmethode mit den beiden früher bei VERA verwendeten Methoden (Gasabsorber- und Degraderfoilmethode) vergleichen zu können.

Die neue Foil stack-Methode vereint die Vorteile beider früheren Methoden. Es konnte sowohl eine hohe Effizienz von 45 %, als auch ein verbesserte Reproduzierbarkeit von unter 0.3 % erreicht werden. Die Reduktion des Hintergrunds auf $^{10}$Be/$^{9}$Be$= 7 \times 10^{-16}$ erlaubt die Messung von Proben mit sehr niedrigem $^{10}$Be-Gehalt. Die neue Foil stack-Methode wird daher in Zukunft die vorher benutzen Messmethoden bei VERA ersetzen.

# Contents

# List of Figures

# List of Tables

# 1. Introduction

## 1.1. The principle of AMS

Accelerator mass spectrometry (AMS) is an highly sensitive technique to detect rare isotopes by single atom counting [Kutschera (1990)]. Typical isotopic ratios measured with AMS are in the range of $10^{-10}$ to $10^{-16}$, which makes many applications in archeology, geology and astrophysics possible. In these fields some applications are exposure dating, radiocarbon dating and determining solar activity in the past.
Typical AMS facilities consist of two mass spectrometers connected via an accelerator. For the measurement, particles of the sample material are sputtered by positively ionized cesium (see section 1.2.1). Some of the sputtered atoms gain an extra electron and can therefore be extracted from the source as negative ions. While traveling through the low energy side of the facility the particles experience their first separation for energy/charge and mass/charge (see section 1.2.2).

The negatively charged ions (including molecules) of the selected mass, are now accelerated towards the positively charged terminal. Inside the terminal the particles are passing through a so-called stripper (foil or gas), where electrons are stripped off. There, molecules are break up and the now positively charged particles are accelerated away from the terminal towards the high energy side of the beam line. Again they are filtered by their energy/charge and momentum/charge before they reach the detector for identification. Detecting $^{10}$Be, the overwhelming background caused by its stable isobar $^{10}$B needs to be suppressed. Since small mass differences as $\Delta M/M \approx 10^{-5}$ cannot be resolved, there needs to be a special separation method. For this, the dependence of energy loss in matter on the atomic number is used[1].

[1]For methods used in the past at VERA see section 1.3.2

The results of the measurements are isotopic ratios, for instance $^{10}Be/^{9}Be$. The count rate of the trace isotope detected by a single ion detector is compared to the abundant isotope measured as a current with a Farady cup. In one measurement series standards with a known isotopic ratio, blanks with a very low isotopic ratio and the samples with the unknown ratio are measured. The measured ratios are normalized to the ratio of the standard material.

Counting atoms in AMS has an advantage over decay counting. It makes it possible to identify the abundance by using less sample material for long-lived radioisotopes with half-lives higher than 1000 a.

## 1.2. The VERA facility

The Vienna Environmental Research Accelerator (VERA) is an AMS-system, consisting of two mass spectrometers (see Fig. 1.1). The so-called low and high energy sides are combined by a pelletron accelerator. Both mass spectrometers consist of electrostatic and magnetic analyzers for energy and momentum separation (see section 1.2.2). To reduce the dispersion of the beam, there are several focusing elements along the beam line:

- Einzel-Lenses
- Magnetic and electrical quadrupole doublet
- Electrostatic analyzers
- Magnetic analyzers

VERA is well situated to measure a wide range of isotopes like $^{14}C$, $^{10}Be$, $^{26}Al$, $^{36}Cl$, $^{41}Ca$, $^{55}Fe$, $^{129}I$, $^{182}Hf$, $^{210}Pb$, $^{236}U$, $^{244}Pu$. Built in 1995 [Kutschera et al. (1997)] it was upgraded with the electrostatic analyzer on the high energy side in 2002 [Vockenhuber et al. (2003)].

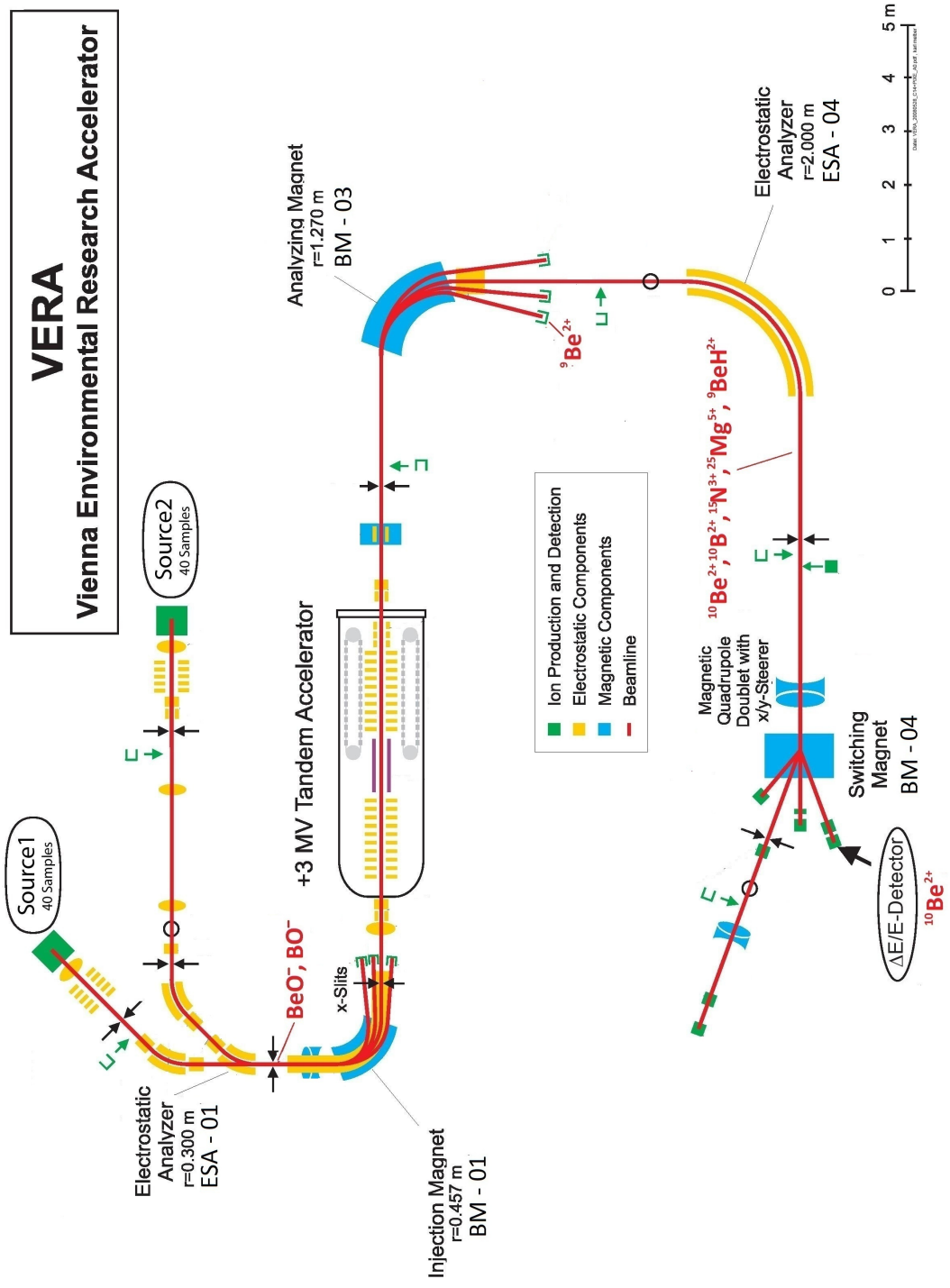


**Figure 1.1.:** This figure shows the main components of VERA in 2012. The nomenclature is with emphasis on measuring $^{10}$Be.

### 1.2.1. Ion source

The ion source at VERA is a so-called "MCSNICS" (Multi Cathode Source of Negative Ions by Cesium Sputtering). Inside the ion source there is a sample wheel which can hold up to 40 target cathodes loaded with sample material. Positively charged cesium ions are attracted by the potential of the sample wheel which lies on -5 kV relative to the source potential.
Particles of the sample material are sputtered and ionized by cesium ions hitting the targets. The now negatively charged sample atoms and molecules are extracted, leaving the source with an energy of about 70 keV. The beam leaving the source is not completely monoenergetic because the ions may retain a variable fraction of energy from the cesium beam. It has to be considered that not every chemical element is able to form negative ions and therefore the ion source can act as a first isobar filter, in some cases. For example nitrogen (N) forms no negative ions, which is important for $^{14}$C measurements. For Be, the yield of $Be^-$ ions is very low, we therefore use BeO mixed with copper as sputter material and inject the molecular ion $^{10}Be^{16}O^-$ into the tandem accelerator as recommended by the Negative Ion Cookbook [Middleton (1990)].

### 1.2.2. Electrostatic and magnetic analyzer

There are two electrostatic analyzers (ESA) and two magnetic analyzers (BM) at VERA, as mentioned in section 1.2.1. One of each kind on the low and on the high energy side. For a charged particle in an electric and magnetic field, the Lorentz force of the form

$$\vec{F} = q(\vec{E} + \vec{v} \times \vec{B}) \tag{1.1}$$

takes effect. Here $q$ is the charge, $\vec{E}$ is the electrical field, $\vec{v}$ is the velocity of the particle and $\vec{B}$ is the magnetic field. Passing through an electrostatic field of the ESA the particle with charge $q$ and mass $m$ experiences a centripetal force according to

$$\left|\vec{F}_C\right| = \frac{mv^2}{r} = q\left|\vec{E}\right| \tag{1.2}$$

The path of the particle is given by its electric rigidity $E_{kin}/q$ according to

$$\frac{\left|\vec{E}\right| r}{2} = \frac{E_{kin}}{q} = const. \tag{1.3}$$

Here $E_{kin}$ is the kinetic energy of the particle. Therefore particles leaving the ESA, have a well defined ratio $E_{kin}/q$. To select a certain magnetic rigidity $p/q$, they are sent through a magnetic field $\vec{B}$ inside the magnetic analyzer. The centripetal force in a magnetic field is given by the second term of Eq. 1.1

$$\vec{F}_C = \frac{mv^2}{r}\frac{\vec{r}}{r} = q\vec{v} \times \vec{B} \tag{1.4}$$

Assuming that the trajectory of the particle is perpendicular to the magnetic field, Eq. 1.5 is valid.

$$rB = \frac{mv}{q} = \frac{p}{q} = const. \tag{1.5}$$

As a consequence, the magnetic rigidity $p/q$ of a particle with mass $m$ is selected by passing a magnetic field with the velocity $v$.

The magnetic analyzer BM-01 on the low energy side is referred to as the injection magnet. The injection magnet is equipped with a multi beam-switcher (MBS). The multi beam-switcher makes it possible to switch between masses in the range of microseconds without changing the magnetic field of BM-01. To vary the mass of the particle that is injected into the accelerator, the velocity of the particle has to be changed. This is carried out by applying a voltage that accelerates the particles in front of the injection magnet. After the injection magnet the particles are decelerated to their initial energy.

The magnetic analyzer BM-03 following the acceleration is used to sort out particles with wrong masses or charge states, chosen for the high energy side. Fragments of the molecules which were broken up in the stripper of the accelerator (see section 1.2.3) will be filtered. After passing the magnetic analyzer one of the Faraday cups measures the current of the abundant isotope while the trace isotope follows the beam line further. Before the trace isotope is detected it passes through the electrostatic analyzer ESA-04 for further energy filtering. After that the switching magnet BM-04 makes it possible to select one of the detection beam lines.

### 1.2.3. Pelletron accelerator

The 3 MV Pelletron accelerator is a 9SDH-2 tandem type from National Electrostatics Corporation (NEC). It works similar to the principle of a Van-de-Graaff generator. The two so-called pelletron chains consist of pellets that are isolated from each other and are used for charge transport to the terminal. After careful conditioning, meaning a slow rise of the terminal voltage[2] over a few days, the terminal can reach a voltage up to 3.6 MV [Steier et al. (2005)]. For insulation the whole structure is located inside a tank filled with $SF_6$ gas (sulfur hexafluoride) at an absolute pressure of about 6 bar. Negatively charged particles are accelerated towards the positive terminal where they are stripped. This stripping of electrons happens when the ions pass either a stripping gas or a stripping foil. For measurements concerning this work $O_2$ was used as a stripping gas. The charge state after stripping is distributed around the mean charge state which depends on the velocity of the ion. A growing areal density leads to an increase of the mean charge state until an equilibrium is reached. Using 3 MV terminal voltage for $^{10}$Be and a pressure of $6.5 \times 10^{-7}$g cm$^{-2}$ of $O_2$ in the 80 cm long stripper tube, we get a charge state yield for 2+ of about 55-60 % while the yield of 3+ ends up to be only about 5-7 % [Martschini (2008)]. The stripping gas gets pumped up at both ends of the stripper tube and is continuously flowing back to the center of the stripper tube.

The now positively charged ions are repelled from the terminal. Their total energy is

$$E_{HE} = \frac{m_{HE}}{m_{LE}}(E_{Inj} + q_{LE} \cdot U_{Acc}) + q_{HE} \cdot U_{Acc} \tag{1.6}$$

where $m_{LE}$ is the mass entering the terminal at the low energy side, $m_{HE}$ the mass of the fragment leaving the terminal, $q_{LE}$, $q_{HE}$ the charge state before and after stripping, respectively $E_{Inj}$ the injection energy, and $U_{Acc}$ the accelerator voltage.

### 1.2.4. Detectors

For particle detection VERA has four dedicated beam lines accessible by the switching magnet BM-04 at the angles $-20°$, $0°$, $20°$ and $40°$. Attached to them are

[2] At VERA there is an automatic conditioning program used that can work unattended.

different types of detectors (Silicon detectors, Ionization chambers, TOF-Detector (Time Of Flight)). To separate isobars like $^{10}$B in our $^{10}$Be measurements, the ionization chamber described in section 3.2 is mounted at the $-20°$ beam line. For detecting $^{14}$C and $^{26}$Al where the stable isobars are already suppressed in the ion source, a silicon detector in front of BM-04 is used to measure the ions total energy and their counting rate, respectively.

## 1.3. AMS of the cosmogenic radionuclide $^{10}$Be

$^{10}$Be has a half-life of (1.387 $\pm$ 0.012) Ma [Korschinek et al. (2010)] and is a naturally occurring radioisotope. It decays via beta decay to the ground state of its stable isobar $^{10}$B. $^{10}$Be is a cosmogenic nuclide produced in spallation processes by cosmic-ray particles in the atmosphere and in-situ in rocks. The production in the atmosphere is mainly on nitrogen and oxygen [Lal (1967)]. In-situ production is caused by fast neutrons on oxygen, silicon and aluminum for example in quartz [Lal (1991)]. Applications of $^{10}$Be measurements vary from exposure and burial dating e.g. [Gosse (2001)] over climate research e.g. [Priller et al. (2004)], [Auer et al. (2007)] to nuclear astrophysics e.g. [Wallner et al. (2008)].

The magnetic field, shielding the earth from cosmic rays, makes the production rate of $^{10}$Be depending on the latitude and on the sun activity. High solar activity leads to a stronger solar magnetic field, which shields the earth from cosmic rays and therefore reduces the production of $^{10}$Be. The same is valid for the magnetic field of the earth. Recent studies by [Christl et al. (2010)] give an average production rate of $^{10}$Be of (1.64 $\pm$ 0.10) $\times$ $10^9$ atoms cm$^{-2}$a$^{-1}$.

### 1.3.1. $^{10}$Be and its isobar $^{10}$B

To measure $^{10}$Be in AMS it has to be separated from the overwhelming background caused by the much more abundant stable isobar $^{10}$B. Because of the high counting rate, caused by $^{10}$B, of about $3 \times 10^6$ *cps* it has to be suppressed before reaching the detector chamber. The small mass difference of $\Delta M/M = 5.97 \times 10^{-5}$ cannot be resolved by the mass spectrometers and therefore the separation of the two isobars is carried out by comparing their energy-loss in matter.
Due to the fact that ions with a larger atomic number have a higher stopping

power[3], it is possible to separate $^{10}$Be from its isobar by guiding the beam through matter. Using SiN-foils in front of the detector guarantees an energy difference before the ions reach the detector[4]. The isobars can then be separated by their difference in energy-loss on the two anodes of the ionization chamber (see section 3.2).
The separation of isobars prior to the detector is limited due to the thickness variations of the foils and the energy straggling in the foils. Energy-loss in matter is caused by atomic and nuclear interactions of the ion with the target material. Most of the energy is lost by electronic stopping (interaction of the ion with the electrons of the target atoms), while only a small number of nuclear interactions take place. As the interaction processes are statistical processes, they lead to a distribution of energy around their mean energy. To reduce the influence of energy straggling the energy should be high.

## 1.3.2. Methods for isobar separation at VERA

At VERA the $^{9}$Be current is measured at a Faraday cup, which is situated after the high energy analyzing magnet BM-03. The measured current of $^{9}$Be is then compared to the $^{10}$Be counts detected at one of the beam lines after the switching magnet BM-04. In the past, two methods were used successfully at VERA to suppress the stable isobar $^{10}$B. The absorber method was implemented by [Priller et al. (2000)], while first measurements with post stripping took place in 2007 [Michlmayer (2007)]. Both methods have their advantages and disadvantages as described below.

### 1.3.2.1. Absorber

The absorber method [Priller et al. (2000)] counts $^{10}$Be with a surface barrier detector, which is placed on the back of a gas cell filled with the absorber gas $CO_2$. As detector entrance window a Titanium-foil is used. To suppress $^{10}$B due to higher stopping power, the pressure of the absorber gas has to be adjusted. It is chosen to be high enough to stop $^{10}$B before it reaches the surface barrier detector while all particles retaining sufficient energy can be detected.

[3]For a more detailed description see section 2.2
[4]In 2010 [Sheng Xu et al. (2010)] used a thick Havar-foil, as an entrance window, to suppress boron at a 5 MV accelerator.

To reduce the influence of straggling in the absorber gas, the initial energy of the isotopes has to be higher than 1 MeV/amu which requires to select the 3+ charge state after the accelerator. This leads to a measured particle transmission of 4.5 % for $^{9}Be^{3+}/^{9}BeO^{-}$ using 3 MV acceleration voltage. The yield of the 2+ charge state would be a factor 10 higher, which makes the necessity of using the 3+ charge state a disadvantage of this method. However, other losses further along the beam line are only around 30 %. The background produced by the $^{10}$B-tail and nuclear reactions in the entrance window are at the level of $^{10}Be/^{9}Be = 10^{-14}$. The reproducibility of results with this method is better than 1 %.

#### 1.3.2.2. Post stripping

For post stripping [Michlmayer (2007)] the ion beam is guided through a foil after the high energy mass spectrometer, followed by another bending element. At VERA, we place a SiN-foil with a thickness of about 500 nm inside beam line 4 between the ESA-04 and the bending magnet BM-04. For this method, the 2+ charge state is selected. After passing through the SiN-foil, the isobars have a small energy difference. This difference is resolved by the switching magnet, where the 3+ or 4+ charge state is chosen. For detection, the compact ionization chamber(see section 3.2) is mounted at the 40° beam line where a $\Delta E/E$ separation takes place.

The measured background of this method of $^{10}Be/^{9}Be < 2 \times 10^{-15}$ is lower and the overall efficiency is higher than using the absorber method. However, significant beam losses after the post stripping foil limit the reproducibility to $\sim 3$ %.

| | degrader foil | gas absorber |
|---|---|---|
| negative ion detection efficiency | 15 % | 5 % |
| reproducibility for samples $^{10}Be/^{9}Be > 10^{-12}$ | 3 % | 1 % |
| background ($^{10}Be/^{9}Be$) | $2 \times 10^{-15}$ | $1 \times 10^{-14}$ |

**Table 1.1.:** Here, the negative ion detection efficiencies, the reproducibility and the background of the degrader foil method and the gas absorber method are listed.

## 1.4. Motivation

As shown above, both the gas absorber and the degrader foil method have significant disadvantages (see Tab. 1.1). Due to the high energy needed for the gas absorber method, the use of the 3+ charge state after acceleration leads to a low transmission. The high background makes this method only suitable for samples with high $^{10}Be/^{9}Be$ isotopic ratios (above $10^{-13}$). The degrader foil method has the advantage of using the 2+ charge state and a low background. The reproducibility however is a disadvantage. The aim of this thesis is to combine the advantages of these methods by using the 2+ charge state and improving the ion optical transmission as well as the reproducibility of results. With the new foil stack method we also hope to reduce the background in the measurements.

# 2. Simulations with SRIM

To separate $^{10}$Be from its isobar $^{10}$B, their different stopping behavior in matter is used. For the measurement very homogeneous SiN-foils were taken that should lead to a complete stopping of the $^{10}$B beam, while $^{10}$Be reaches the detector-chamber. To find the optimum areal density of SiN, simulations had to be done. The program used for the simulations was SRIM.

## 2.1. Description of SRIM/TRIM

SRIM (Stopping and Range of Ions in Matter) [Ziegler J.F., Biersack J.P., Ziegler M.D. (2008)] is a program based on the Monte Carlo simulation method. With its core program TRIM (Transport of Ions in Matter) it is a helpful tool to determine the range of ions in matter for individual settings. A screenshot of the program is shown in Fig. 2.1. The input needed is the energy, the type of the ion and the target material. A typical output-file used to determine the behavior of $^{10}$Be moving through a 1000 nm silicon-nitride-foil can be seen in Appendix B. Here the energy, the lateral position and the direction of the ion after passing a certain depth of matter are listed. For a more detailed description see [Ziegler J.F., Biersack J.P., Ziegler M.D. (2008)].

## 2.2. Energy-loss of ions in matter

The main focus of the simulations was the energy-loss of $^{10}$Be and $^{10}$B ions in SiN. Ions passing through matter lose their energy by ion-electron interaction, ion-nucleus interactions, electron uptake or loss and, for high energies, in nuclear reactions. This leads to an energy transfer from ions to the target material. The definition of the stopping cross section S, which describes the mean energy loss,

is given by

$$S = -\lim_{N\Delta x \to 0} \frac{\langle \Delta E \rangle}{N\Delta x} = -\frac{dE}{Ndx} \tag{2.1}$$

Here $\langle \Delta E \rangle$ is the particle's energy loss while passing the areal density $N\Delta x$.
The most common model to describe the stopping power is the Bethe Bloch formula shown in Eq. 2.2.

$$S = \frac{4\pi Z_1^2 e^4}{m_e v_1^2 (4\pi\epsilon_0)^2} Z_2 \left[\ln \frac{2m_e v_1^2}{I}\right] \tag{2.2}$$

with $Z_1$ and $Z_2$ being the atomic number of the projectile and the target, $v_1$ the velocity of the projectile, I the ionization potential and $m_e$ the electron mass. For relativistic velocities $\beta = v/c$ has to be considered in the Bethe Bloch formula. In our measurement $\beta$ reaches only $\sim 4\%$ and can therefore be neglected.
The equation shows that the stopping power is proportional to $Z_1^2$ resulting in a higher energy loss for higher atomic numbers. For example, B with an atomic number of 5 loses more energy and is therefore stopped earlier than Be with an atomic number of 4 as shown in Fig. 2.2. Strictly Eq. 2.2 is only valid if the energy of the projectile is high enough that all electrons are stripped off. For lower energies, as used for our applications the projectile is not fully stripped any longer and electrons will partly shield the nucleus. Therefore $Z_1$ in Eq. 2.2 has to be replaced with a lower effective charge $Z_{eff}$ which is still a function of $Z_1$.

## 2.3. Simulations

The goal of the simulations was to find the areal density needed for a sufficient suppression of the boron background. $^{10}$B should be stopped in a foil stack of silicon nitride-foils (SiN) while the energy of $^{10}$Be is high enough to reach the second anode of the ionization chamber[1] (see Fig. 2.2). The foils with $5 \times 5$ mm$^2$ windows, a frame size of $10 \times 10$ mm$^2$ and a nominal thickness of 1 $\mu$m are all from the same batch containing 20 foils, supplied by [Silson Ltd (2012)][2]. These foils are very homogeneous, which is a requirement for good measurement.

The main parameters are the energy of the incident ion, the areal density of the

[1] described in section 3.2
[2] Foils from [Silson Ltd (2012)] are supplied from 30 nm to 1 $\mu$m thickness.

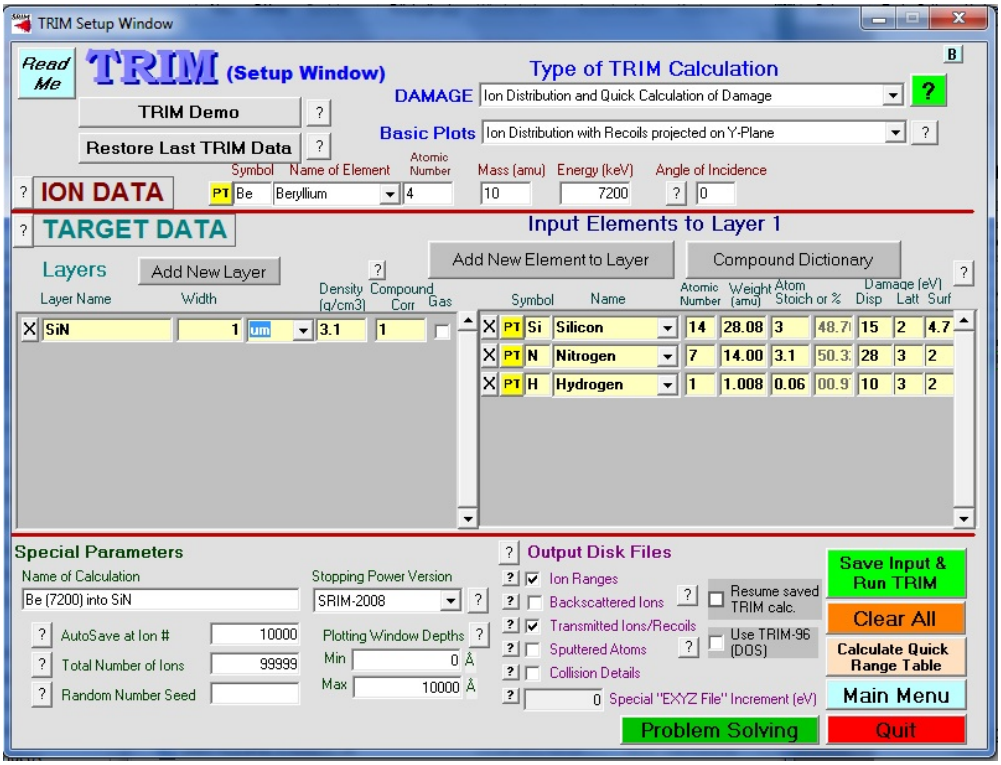


**Figure 2.1.:** Screen shot of SRIM/TRIM setup window. In the upper part the energy and the ion type can be selected. In the middle on the right there are the layers listed where an areal density (in the form of thickness and density) of the target material is entered. The compound of the layer can be seen on the right. The fields on the bottom make it possible to choose the ion number and the kind of data that should be generated in the output file.

foils and their composition. With a density of 3.1 g/cm$^3$ [Döbeli et al. (2004)] the nominal areal density for one foil is 310 $\mu$g/cm$^2$. The compound composition of the SiN-foils was taken from [Döbeli et al. (2004)] and is $Si_3N_{3.1}H_{0.06}$. We want to take advantage of the high yield for the 2+ charge state, measuring with 3 MV terminal voltage at VERA. The energy of the ions on the high energy side can be calculated with Eq. 1.6 leading to an energy of 7.18 MeV for detection of $^{10}Be^{2+}$ ions injected with an energy of 70 keV as $^{10}Be^{16}O^-$ molecules. Entering these parameters in SRIM, we get the residual energy of the ions passing the SiN-foils, depending on the areal density.

The loss of ions by angular straggling is also a parameter which had to be considered. For this the whole foil stack had to be simulated. This rather complex procedure is described in the next subsection.

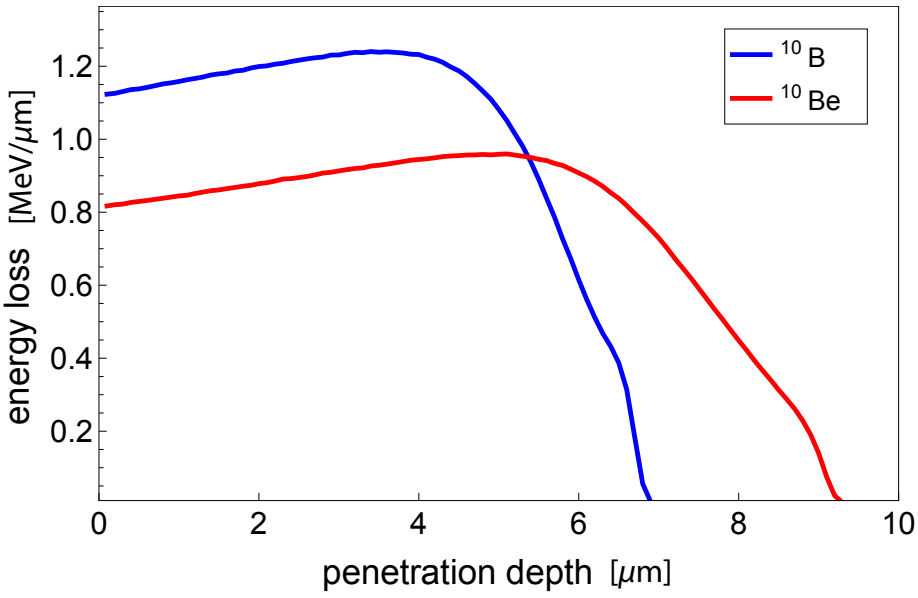


**Figure 2.2.:** Energy loss curves of $^{10}$Be and $^{10}$B ions in SiN with an initial energy of 7.2 MeV according to SRIM. The compound composition of SiN used for the simulations was $Si_3N_{3.1}H_{0.06}$ [Döbeli et al. (2004)]. It can be clearly seen that at a certain penetration depth $^{10}$B with a higher atomic number is stopped, whereas $^{10}$Be has some residual energy.

### 2.3.1. Simulation of the foil stack

Simulating the foil stack allows to estimate the number of ions lost within the foils by angular straggling. While the foils are very thin (1 $\mu$m), they are separated by much bigger gaps (1 mm) of vacuum. If an ion gets scattered inside the foil, it is possible that the angle at the exit is large enough that it can not enter the next foil and is therefore lost. As the energy of the ions gets lower, the straggling and therefore the possibility of ion loss increases. Fig. 2.3 shows two screenshots of the simulated foil stack.

In SRIM there is a problem with simulations of layers with very different thicknesses in one step caused by inappropriately chosen step sizes for the thin layer (in our case the SiN-foils). This results in the fact that each foil and each gap between them has to be simulated separately.

The foil stack consists of up to 14 SiN-foils. There is a 1 mm spacing between them and a 3 mm gap separating the last foil from the entrance window of the detector chamber. After simulating one foil, the SRIM output gives the new lateral posi-

tion in x- and y- direction and the ion's direction. This data has to be extracted to calculate the ion path in the vacuum. For simulating the next foil, the data has to be imported back into SRIM. Therefore, the path of the ion through each foil has to be simulated separately. To simulate the whole foil stack, 14 foils with vacuum between them, the Mathematica-routine "Auto-SRIM", written by Josef Buchriegler[3], was used. It automated the simulations with varying foil numbers and different ions by manipulating the SRIM in- and outputs. Ions entering the foil stack are not mono-energetic, thus the energy-distribution fed into the program is a Gaussian.
The spread of the beam was according to [Martschini (2008)] 3.0 mm FWHM[4] in width and of 1.8 mm FWHM in height, observed at the image slits of ESA-04. "Auto-SRIM" can also simulate the ionization chamber, where the number of anodes as well as their length can be adapted. The input parameters have to be written into a text file, as shown in Appendix A. Input parameters range from foil quantity, foil distance, ion type, ion energy and diameter of the beam to the number of anodes in the detector chamber.

## 2.4. Outcome of the simulations

First simulations turned out to be quite easy. But performing the first measurements revealed many new findings that lead to many more simulations and in addition to the measurement of the areal density of the SiN-foils in the foil stack described in section 3.5.

### 2.4.1. Discrepancies in the areal density

After performing the first simulations a need of about 8 SiN-foils with a nominal thickness of 1 $\mu$m [Silson Ltd (2012)] was estimated to suppress $^{10}$B with minimum loss of $^{10}$Be (see Fig. 2.2). This corresponds to an areal density of 2480 $\mu g/\mathrm{cm}^2$. Performing first measurement revealed that the $^{10}$B ions have not lost enough energy after 8 foils. For this measurements the terminal voltage had to be dropped down to 1.8 MV to suppress $^{10}$B sufficiently. This is equivalent to an ion energy

[3][Buchriegler, J. (2013)]
[4]Full Width Half Maximum

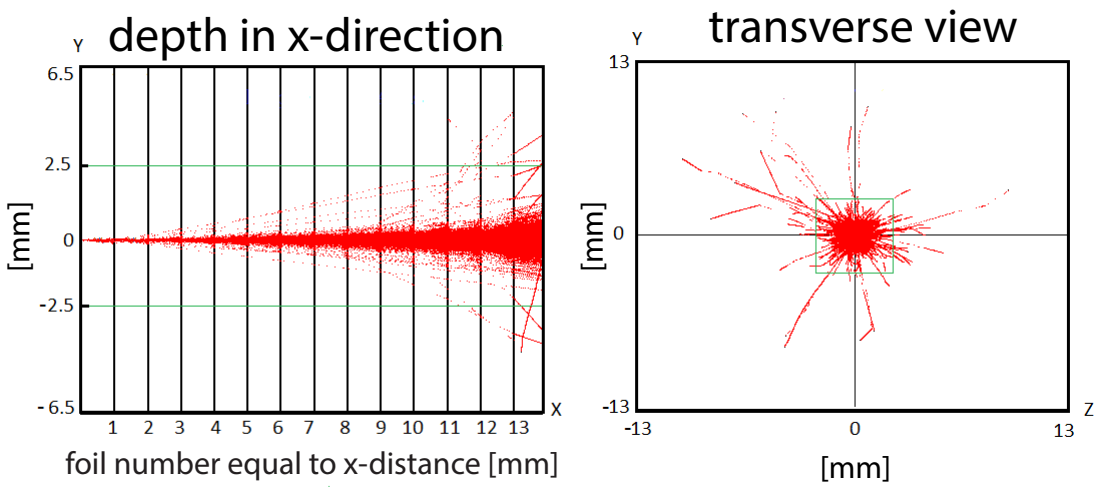


**Figure 2.3.:** This figure shows a simulation done with SRIM. The $^{10}$Be beam was sent through 13 foils of SiN separated by 1 mm vacuum. It can be seen that for higher foil numbers the angular straggling increases while the energy decreases. The vertical lines in the left picture indicate the foils. The green lines in the left figure and the green square in the right figure indicate the size of the foils.

of only 4.31 MeV. We decided to use more foils because using a higher ion energy leads to a lower influence of energy loss straggling and is expected to yield a better separation. After more measurements with different numbers of foils we found the optimum to be 13 foils. This implies a nominal areal density of 4030 $\mu g/\mathrm{cm}^2$. With this number of foils we were able to use a terminal voltage of 3.0 MV corresponding to an ion energy of 7.18 MeV. The nominal areal density clearly contradicted the results of the initial simulations and requires further analysis.

### 2.4.2. Final simulation parameters

The final simulations started off to be challenging because of the uncertainties concerning the areal density described in section 3.5. In the following the final simulation parameters, that were used to compare the measured data with the simulations and to identify possible background appearing in the measurements (see section 4.2.1) are discussed.

$^{10}$Be was sent into SiN-foils with an mean energy of 7.209 MeV. The composition

of SiN was (see section 2.3) $Si_3N_{3.1}H_{0.06}$. 13 foils with a thickness of 446 nm each[5] and a window with a thickness of 100 nm were used to get an areal density of 1900 $\mu g/cm^2$ for the simulations. The broadening of the beam with a diameter of 2.4 mm (FWHM) was given by the mean value between the beam's divergence in height and width determined by [Martschini (2008)]. The beam widens along the foil stack to a diameter of 3.3 mm (FWHM) and leads to a negligible ion loss of 0.4 % by angular straggling in the simulations.
These simulations led to a stopping of $^{10}B$ in the foil stack while $^{10}Be$ has a mean residual energy of 934 keV after passing through the foil stack and the entrance window of the ionization chamber.

[5]Based on the measured residual energy of $^{10}Be$ entering the detector.

# 3. Materials and methods

The $^{10}Be^{2+}$ ions were detected using an ionization chamber. With the split anodes of the chamber it is possible to identify ions by their energy-loss in a two-dimensional spectrum. SiN-foils were placed in a foil stack holder right before the entrance window of the detection chamber. Therefore it was necessary to construct a holder, that had to meet certain criteria, which are presented in this chapter. Furthermore the areal density of the foils had to be determined experimentally to resolve differences between measurements and simulations.

## 3.1. Construction of the foil stack holder

The separation of $^{10}B^{2+}$ and $^{10}Be^{2+}$ is induced by an energy dispartment in SiN-foils placed in front of the window foil of the detector. To put the foils as close as possible to the window-foil, we built a holder, which directly fits into the detector window holder as shown in Fig. 3.1.

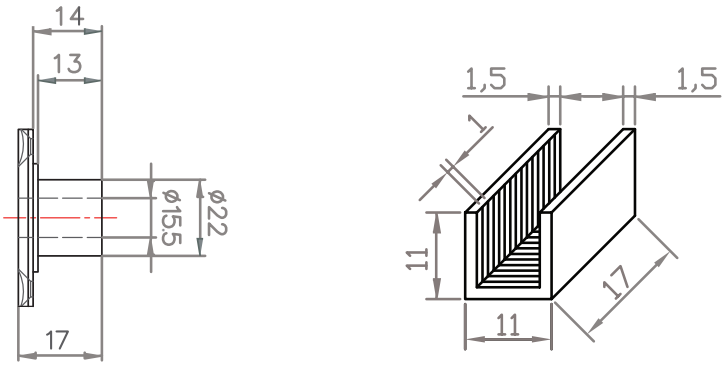


**Figure 3.1.:** The left figure shows the construction plan of the window holder in black. Red indicates the beam. The foil stack holder that goes into the window holder is shown on the right. It can be slid into the window holder filled with up to 14 foils separated by 1 mm gaps. Written in gray are the dimensions in millimeters

For the construction, several points had to be considered:

- If the foils get in contact with each other they are destroyed. Hence the foils should have gaps between them.
- The last foil should be as close as possible to the entrance-window to keep the ion loss by angular straggling small.
- The size was limited by the surroundings, so the holder had to be small enough to fit into the already existing window opening and big enough to hold the 10 $\times$ 10 mm$^2$ frames of the foils.
- To be flexible, the holder should be able to hold as many foils as possible. Therefore we used the whole length of the window holder.
- It was required to be easy to handle and fast to mount.

The finished holder can be seen in Fig. 3.2. It is made of aluminum and is able to hold up to 14 SiN-foils with a frame size of 10 $\times$ 10 mm$^2$. Fig. 3.3 shows a cross section of the detection chamber with the foil stack placed in front of the entrance window of the detector.

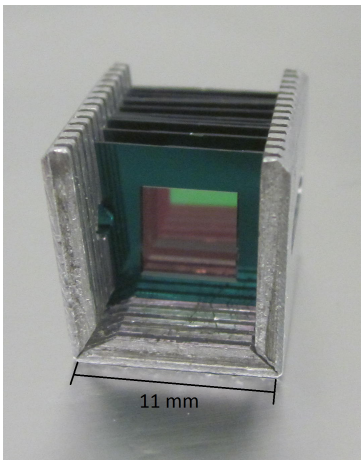


**Figure 3.2.:** Picture of the foil stack holder filled with 8 SiN-foils.

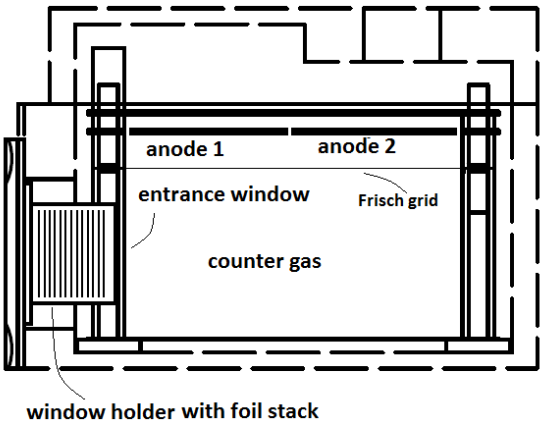


**Figure 3.3.:** This figure shows a cross section of the ionization chamber. The split anodes can be seen on the top. The foil stack in the window holder is indicated as 13 black stripes. After the foil stack there is the 100 nm thick SiN-entrance window which separates the counter gas from the vacuum in the beam line. The dashed lines indicate the casing.

## 3.2. The ionization chamber detector

The ionization chamber shown in Fig. 3.3 has a $5 \times 5$ mm$^2$ SiN-window[1] with a thickness of 100 nm. The purpose of this window is to separate the counter-gas inside the detection chamber from the vacuum in the beam line. In Fig. 3.5 it can be seen that the chamber is fixed on the lower end of a feed through. This makes it possible to remove the chamber from the beam path without breaking the vacuum. Inside of the detector box, there are two anodes, one in the front and one in the rear section of the detector. Each anode is connected to a preamplifier. As counter-gas, isobutane is used. The pressure of the isobutane-gas inside the detector can be held on a constant level by regulating the gas flow with a valve. In front of the chamber, there are two apertures (3 mm and 6 mm) which can be selected to be put into the beam path. The apertures and the detector are mounted on individual feed throughs at a cross pipe and can be retracted separately. This makes it possible to use the apertures for tuning with another detector which can be mounted behind the ionization chamber.

[1]For other applications the window size and thickness can be adapted

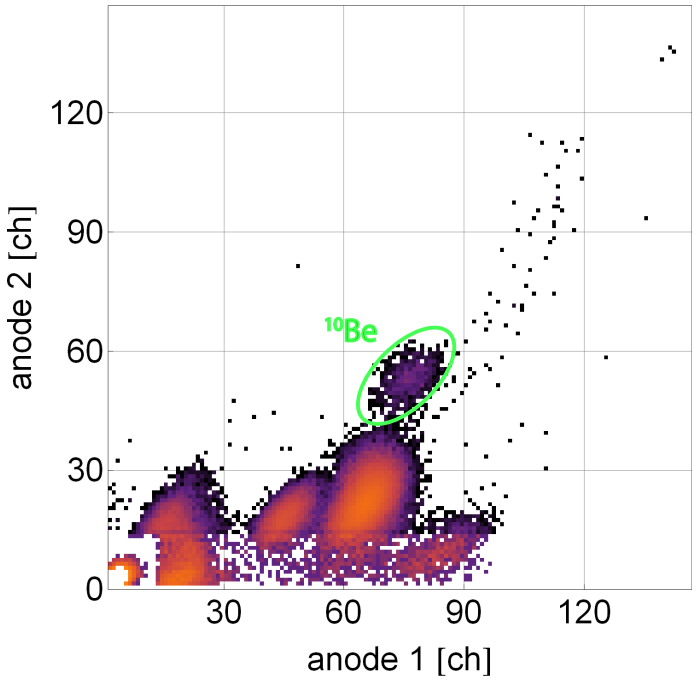


**Figure 3.4.:** This figure shows an example of a two-dimensional spectrum. Plotted on the abscissa is the energy-loss on the first anode and plotted on the ordinate is the energy loss on the second anode, both in unit of channels which are exported by the ADCs. Peaks shown in this spectrum are explained in chapter 4.

There are three possibilities for an ion that has entered the ionization chamber to be detected and they depend on the gas pressure in the chamber, the stopping power and the energy of the ion. First, an ion entering the ionization chamber can lose its whole energy on the first anode. This gives us the total energy of the ion if we consider the energy lost in the entrance window. Second, the ion can also be stopped at the second anode. Here we get the total energy if we sum up the energy-loss on both anodes. Third, it is not possible to determine the ions energy if the ion passes through the detector and hits the rear wall of the detector chamber.

$^{10}$B with a higher energy-loss in matter can be stopped at the first anode and then be separated from $^{10}$Be which is stopped at the second anode. But because of the high count rate caused by the stable $^{10}$B, it has to be suppressed before it reaches the detector chamber.

The result of evaluating the energy-loss on both anodes is a two-dimensional spectrum shown in Fig. 3.4. Here, the abscissa shows the energy-loss on the first anode

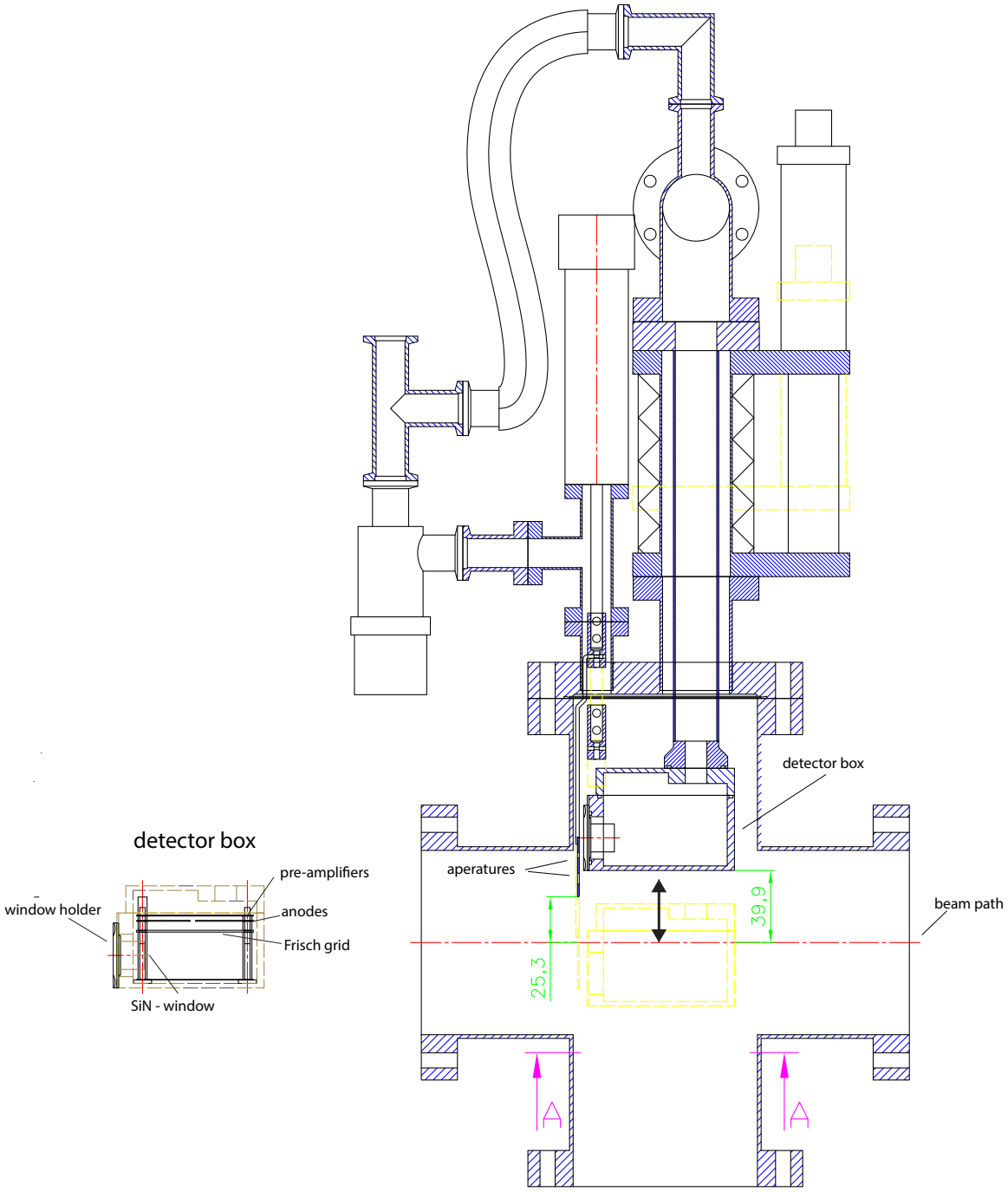


**Figure 3.5.:** This ionization chamber detector built by Oliver Forstner [Forstner et al. (2008)] was based on the design from ETH Zürich [Döbeli et al. (2004)]

and the ordinate the energy-loss on the second anode. The units on the axes are channels. Each channel in the ADCs (Analog Digital Converter) corresponds to a certain energy interval. To assign the energies to channels an energy calibration had to be performed.

## 3.3. Energy calibration

After detecting an ion in the ionization chamber, the signals from both anodes are fed into ADCs. The digital signal reaches the MCA[2] where it is sorted according to its pulse height. Each height corresponds to a channel in the ADC. For the energy calibration, $^{10}$B with an energy of 6.9 MeV was detected without a foil stack and, because of different amplification factors, the pressure of the isobutane-gas in the ionization chamber was varied from 85 mbar to 107 mbar. With a constant gain[3] at the amplifiers the $^{10}$B-peak was traced in the energy spectrum. For this $^{10}$B had to be fully stopped in the ionization chamber. The total energy of $^{10}$B lost on both anodes and therefore the peak position should be constant. The mean channel, where the peak of $^{10}$B with an energy of 6.9 MeV was detected lies in channel $(448 \pm 4)\,ch$. Taking into account various uncertainties of this method (e.g. the extrapolation to the significantly lower gas pressure) this corresponds to $(6.1 \pm 0.3)$ keV/ch for the final settings of the electronics.

## 3.4. Beam tuning

Whereas the disadvantage of the high $^{10}B^{2+}$ count rate results in a detection challenge of $^{10}Be^{2+}$, the advantage is that it provides a current of a few pA and can be used for beam tuning. To implement this method, Faraday cups along the analyzer beam line are connected to SRS[4] SR570 current amplifiers, characterized by their high sensitivity. The $^{10}B^{2+}$ beam is then tuned through the high energy side to hit a Faraday cup located right behind the ionization chamber. To bring the beam to the spot where it could enter the ionization chamber, a 3 mm aperture

[2]Multichannel Analyzer
[3]The gain at the amplifiers was set with a pulser to the same pulse-height leading to a different gain for each anode which was considered in the calculations.
[4][Stanford Research (1980)]

is inserted into the beam line while the ionization chamber stays retracted. The beam is than tuned onto the Farady cup through the 3mm aperture. After using the program AUTOMAX [Steier et al. (2000)] to maximize the current on the Faraday cup through the aperture, the ionization chamber can be inserted back into the beam line. To expose the whole $5 \times 5\,\mathrm{mm}^2$ opening of the foil stack, the aperture is removed throughout the measurement. Due to the low mass difference of $^{10}B^{2+}$ and $^{10}Be^{2+}$ of $5.97 \times 10^{-4}$ their beams are horizontally spread by 0.14 mm at the detector position. This small offset could be neglected because of the small beam width compared to the size of the SiN-foils. The benefit of this tuning method is the possibility of a straight forward beam tuning.

## 3.5. Measurement of the areal density of SiN-foils

The experimental determination of the areal density was crucial to identify the differences between simulations and measurements discussed in section 2.4. To generate an alpha source, the radioactive compound $^{220}Rn$ from the Thorium series was brought onto a nail in a Hahn emanatorium. Together with the foil that

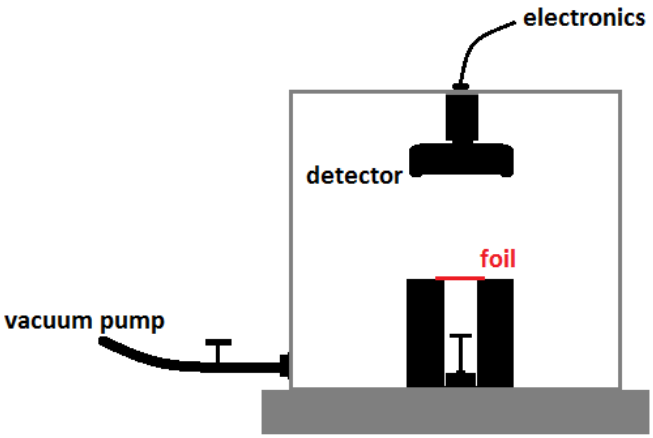


**Figure 3.6.:** Schematic drawing to visualize the measurement of the areal density. Grey: The whole setup is covered by a lid so that vacuum can be generated. Black: On the top and on the bottom left side one can see where the electronics and the vacuum pumps are attached. The foil of which the density is measured is drawn in red. Underneath the foil the nail with the radioactive compound is inserted. Around the nail a hollow cylinder is placed just to hold the foil. In a distance of about 3 cm the Silicon-semiconductor detector is mounted.

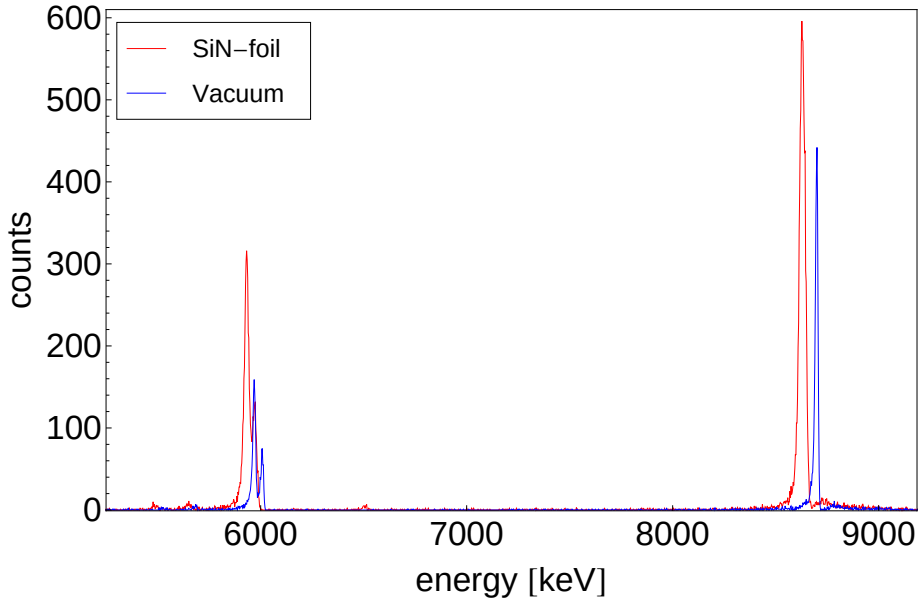


**Figure 3.7.:** Both spectra shown in this figure are produced by alpha particles. Blue is the spectrum of the energy calibration and reference measurement. Red (Due to the longer measurement period the signal is higher) is the measurement with foil nr. 4 (Fig. 3.8). The energy difference for this foil is $(145 \pm 1)$ keV corresponding to an areal density of $(313 \pm 4)\,\mu g/\mathrm{cm}^2$

should be measured, it was then put into the detection assembly (see Fig. 3.6). For detection of the alpha particles, a silicon-semiconductor detector was used. The pressure during the measurement was $5 \times 10^{-2}$ mbar. The energy of the alpha particles was recorded after they passed through the foil. To evaluate the data an energy calibration had to be performed. This was derived from a measurement in vacuum without any foil. With the knowledge of the alpha energies in the Thorium-series the energy calibration was simple. Three alpha-lines were detected. Two at the energies of 6.051 MeV, and 6.090 MeV respectively from the decay $^{212}\mathrm{Bi} \rightarrow ^{208}\mathrm{Ti}$ and one at 8.784 MeV from $^{212}\mathrm{Po} \rightarrow ^{208}\mathrm{Pb}$. The energy calibration was done by assigning the energies to the channels where the maxima of the lines lie. The spectrum of the energy calibration measurement can be seen in blue in Fig. 3.7. The red spectrum in this figure shows a measurement in the vacuum with one foil. From the energy displacement the energy-loss of the alpha particles in the SiN-foil can be derived. To calculate the areal density, the electronic stopping is divided by the energy-loss. The values for electronic stopping power of an $\alpha$ in

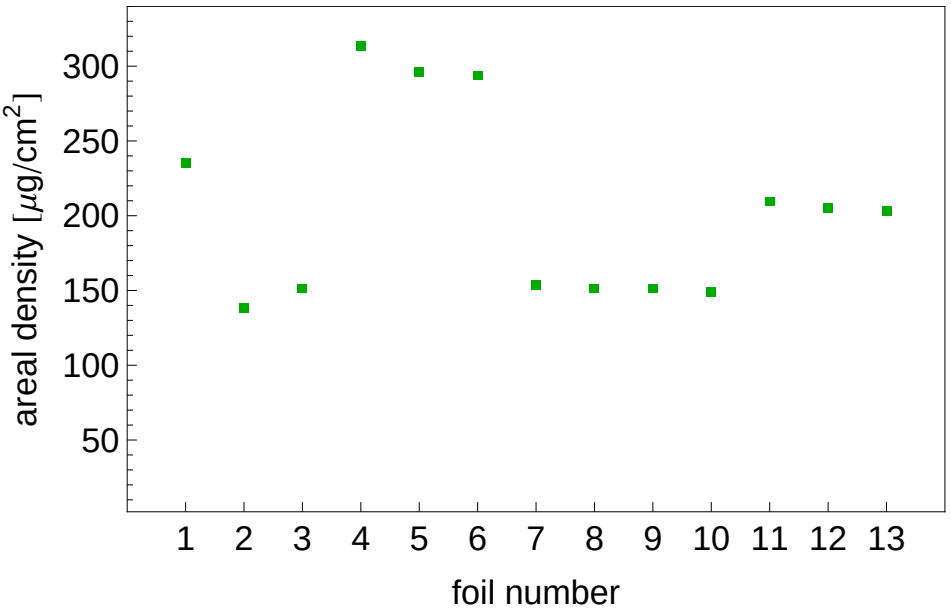


**Figure 3.8.:** This Figure shows the areal densities of all 13 foils used for our measurements. The foil position is according to their position in the foil stack. The uncertainties in areal density are smaller than the actual markers.

SiN were taken from the SRIM database.

In Fig. 3.8 the areal densities for all foils are plotted. The foil number is according to their position in the foil stack[5].. It is visible that the areal density variates strongly from the nominal $310\,\mu g/\mathrm{cm}^2$ to a very low $(149 \pm 3)\mu g/\mathrm{cm}^2$. Summing up all the foils we get a total areal density of $(2650 \pm 50)\,\mu g/\mathrm{cm}^2$. Comparing this to the estimated value of $2480\,\mu g/\mathrm{cm}^2$ after the first simulations we find that the values are in reasonable agreement.

[5]Nr.1 is hit first by the beam running through to nr.13 right before the entrance window

# 4. Results

To determine the possibilities of the foil stack method several measurements were performed at the VERA laboratory. For the finding of the optimum setup three different standards and one $^{10}$Be-free blank were measured. By remeasuring environmental samples the accuracy of the foil stack method was confirmed. Also unknown samples from a new project were measured and compared to the results from the DREAMS facility in Dresden. The most likely origin of background in the measurements was identified by performing simulations.

## 4.1. Measurements at VERA

After several measurements the difficulties concerning the nominal areal density of the SiN-foils, described in section 2.4.1, could be solved. With the optimum setup described below the measurements of the standard materials as well as the blank material could be applied.

### 4.1.1. Measured materials

For the measurements three different standards and one very low blank were available. The SMD-Be-12 standard has a nominal value of $^{10}\mathrm{Be}/^{9}\mathrm{Be} = (1.70 \pm 0.03) \times 10^{-12}$ [Akhmadaliev et al. (2012)]. The in-house ATI-Be[1] standard with a similar value of $^{10}\mathrm{Be}/^{9}\mathrm{Be}=(1.72 \pm 0.05) \times 10^{-12}$ was derived from a BeO irradiated with neutrons at the "Atominstitut" of the University of Technology, Vienna. The third standard, S555 produced at ETH-Zürich has a very high isotopic ratio of $^{10}\mathrm{Be}/^{9}\mathrm{Be} = (8.71 \pm 0.26) \times 10^{-11}$ [Alimov et al. (2009)]. The blank

[1] Further measurements of this standard material showed variations in the ratios. This standard material seems to be inhomogeneous and is therefore not reliable.

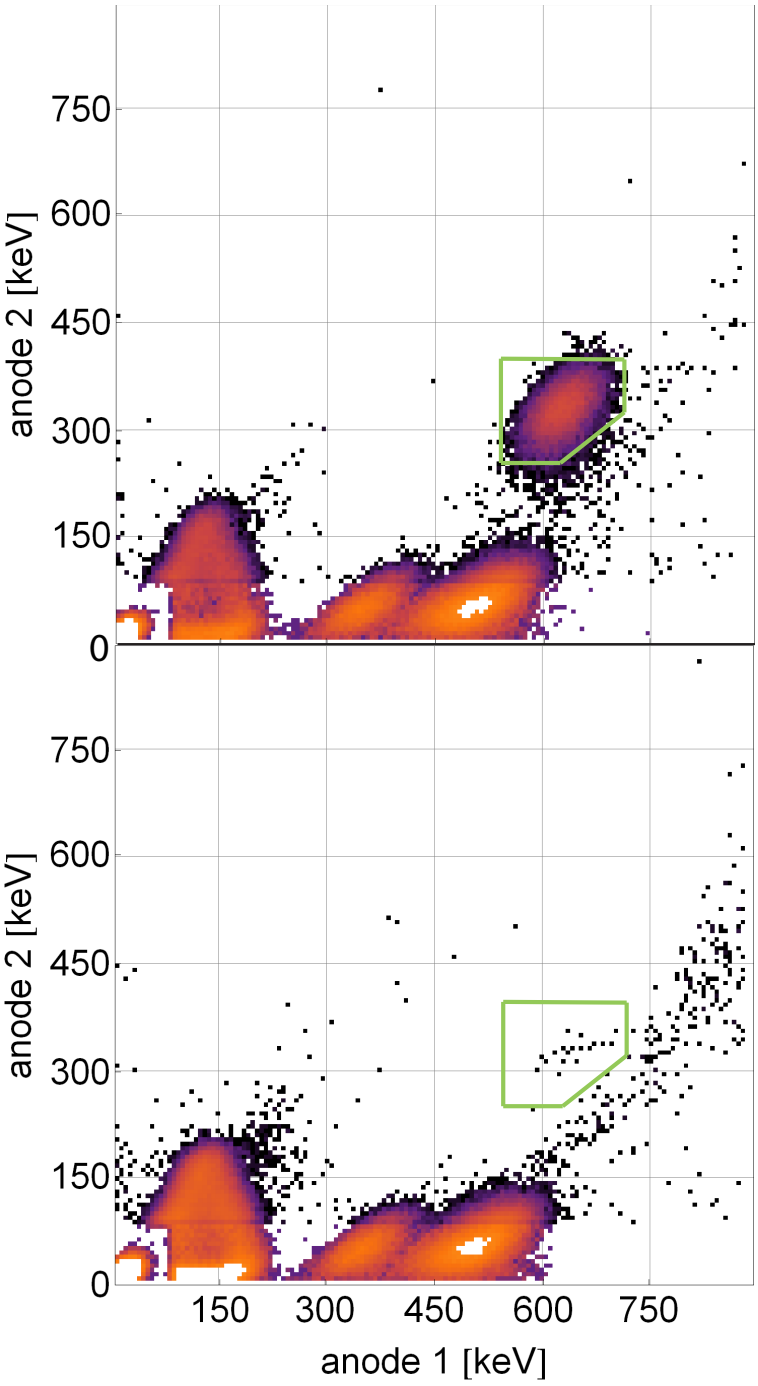


**Figure 4.1.:** This figure shows two-dimensional energy-loss spectra of the ATI-Be standard (upper figure) and the Phenakite blank (lower figure). Framed in green is the $^{10}$Be region of interest. The acquisition time of the standard was $\sim$4 min whereas the acquisition time of the blank was $\sim$60 min. Below channel 15 only every 100$^{st}$ event is detected therefore the content of these channels was multiplied by 100. The peaks of the spectra were identified by simulations (see Fig. 4.3).

material was prepared from Phenakite ($Be_2SiO_4$) a rare crystal. This material has the lowest $^{10}Be/^{9}Be < 10^{-15}$ [Merchel et al. (2008)] ratio known.

In addition environmental samples were measured, which are described in section 4.3. For this we had the possibility to remeasure samples from applications described in [Priller et al. (2004)] and [Auer et al. (2009)] that have been measured in the past at VERA with other methods. Finally, marine core samples of unknown $^{10}Be$ content were measured with the foil stack method for the dissertation of Mag. Jenny Feige.

### 4.1.2. Detection of $^{10}Be$

Several measurements were performed to find the ideal suppression of $^{10}B$ while using the highest terminal voltage possible. The final settings for the measurements were a terminal voltage of 3.0 MV with 13 foils in the foil stack holder. To stop the $^{10}Be$ completely in the ionization chamber, the pressure of the isobutane-gas was 17 mbar. In Fig. 4.1 there are two $\Delta E/E$ spectra that show a standard as well as a blank measurement. The acquisition time for the blank measurement was $\sim$60 min, fifteen times longer than the standard measurements. Marked in green is the bin where the counts are identified as $^{10}Be$. Apart from a weak tail the $^{10}Be$ peak in the standard material is well separated from the background[2]. In the $^{10}Be$ bin of the blank material there are a few counts detected. Because of their distribution similar to the shape of the $^{10}Be$ peak in the standard material these 18 counts are expected to be mainly $^{10}Be$ corresponding to an isotopic ratio of $(7.1 \pm 1.7) \times 10^{-16}$.

### 4.1.3. Detection efficiency and reproducibility of results

To avoid cross contamination in the ion source from the high S555 standard onto the blank material we measured this material after all blank measurements were completed. In Fig. 4.2 the measured isotopic ratios of five S555 sputter targets are displayed. For the chosen bin the mean of the absolute isotopic ratios is $^{10}Be/^{9}Be = 6.98 \times 10^{-11}$, indicated by the blue line in Fig. 4.2. This is 20 % lower than the nominal value of the standard (see section 4.1.1) resulting in a detector

[2]The origin and identification of the background is discussed in section 4.2.1

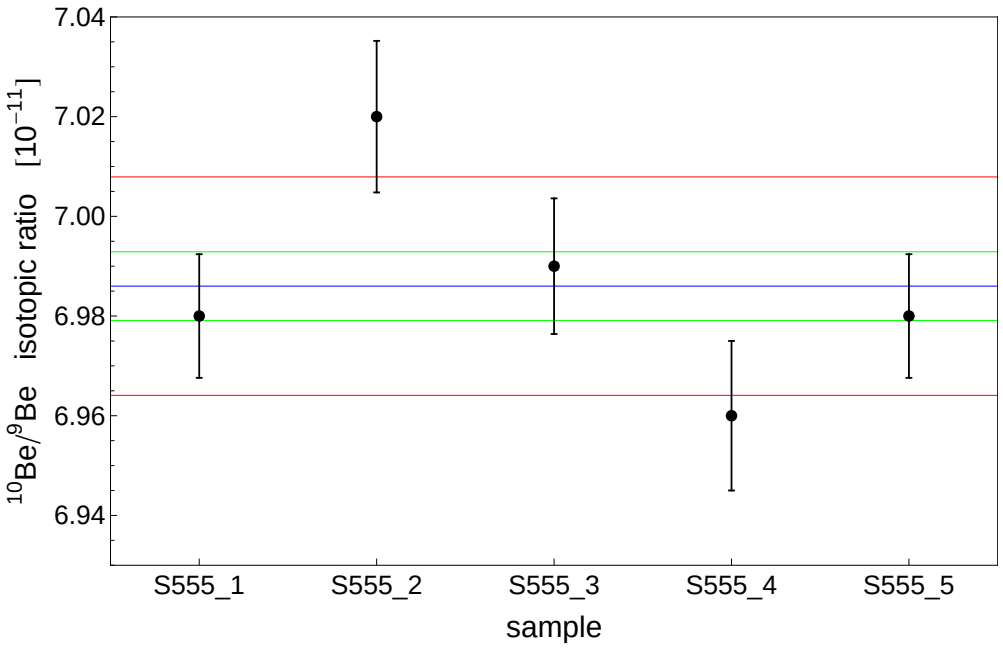


**Figure 4.2.:** This figure shows the absolute isotopic ratios of five S555 standard samples. The error bars are given by the statistical uncertainty. The red line indicates the standard deviation (0.3 %) and the green line indicates the uncertainty of the mean (0.1 %)

.

efficiency of 80 %. The detector efficiency can be raised to 90 % by choosing a larger bin. The origin of the remaining losses is unknown but could probably be caused by fractionation in the ion source, the stripping process, different ion optical transmission or losses in the foil stack by angular straggling. The results of the S555 measurements were taken for the determination of the reproducibility. With respect to the uncertainty all samples lie within one standard deviation, which results in a reproducibility better than 0.3 %. Due to the high efficiency the foil stack method leads quickly to good statistic.

## 4.2. Comparison of experimental results with simulations

Fig. 4.3 gives a comparison of the simulations with the outcome of the measurements. In gray it shows a two-dimensional energy spectrum composed of three measured materials, Beryllium-Oxide, ATI-Standard and a Phenakite-Blank. The

colored lines and dots are results of the simulations with SRIM. In this section the background is identified by evaluating SRIM simulations.

### 4.2.1. Identification of the background

With uncertainties in the areal density of the SiN-foils described in section 2.4.1, discrepancies in the energy-loss appeared when the nominal areal density was used for the simulations. Hence, to compare the simulations with the measurements

| ion | from energy [MeV] | to energy [MeV] | detection |
|---|---|---|---|
| $^{1}$H | 0.050 | 1.80 | yes |
| $^{4}$He | 1.00 | 13.33 | yes |
| $^{7}$Be | 6.50 | 8.13 | yes |
| $^{7}$Li | 4.00 | 7.50 | no |
| $^{10}$Be | - | 7.21 | yes |
| $^{10}$B | - | 7.21 | no |
| $^{11}$B | 7.10 | 12.00 | yes |
| $^{12}$C | 4.60 | 15.56 | maybe |
| $^{14}$N | 10.76 | 10.84 | yes |
| $^{16}$O | 6.75 | 16.75 | maybe |
| $^{25}$Mg | 17.00 | 18.02 | yes |
| molecule | ion | energy [keV] | detection |
| $^{9}$Be$^{1}$H$^{2+}$ | $^{9}$Be | 6.48 | yes |
| | $^{1}$H | 0.72 | yes |

**Table 4.1.:** The table shows all the ions that were simulated. Most ions were simulated over the full energy range. Given in this table is the energy of the ions entering the first SiN-foil. The right column indicates if the simulated ion was identified in the measured spectrum. The last two rows list the parameters of the molecule with mass 10 that can be expected. The molecule was broken up in the first SiN-foil which would lead to the maximum energies listed. The simulations were made with an areal density of 1900 $\mu g/cm^2$ and an isobutane-gas pressure of 13.5 mbar (see section 4.2.1).

and identify the background, the areal density was adapted. For this, a reference point was needed. Because the $^{10}Be^{2+}$ peak in the two-dimensional spectrum was clearly identified, its location in the spectrum was chosen to be the reference point for the simulations.
The energy of the reference point was given by adding up the energy-loss of both anodes. Therefore the mean total energy of $^{10}Be^{2+}$ entering the ionization chamber is $(936 \pm 47)$ keV. The simulated $^{10}Be^{2+}$ ions were sent into the first foil with a mean energy of 7.21 MeV. In the simulations, the areal density of all 13 foils including the entrance window was adapted such that the mean ion energy after the window foil was 936 keV. This was accomplished by usin an areal density of $1900\,\mu g/cm^2$.
To match the simulated ions to structures in the spectrum the energy-loss on each anode was also of interest. For this the pressure of the isobutane-gas in the simulations had to be adjusted. The gas pressure for measuring the spectrum in Fig. 4.3 was reduced to 13 mbar to allow more ions to reach the second anode, which simplifies identification. For $^{10}Be^{2+}$ 13 mbar leads to an energy-loss of 449 keV on the first anode and 334 keV on the second anode. For the simulations the pressure of the isobutan gas was adapted until the energy loss of $^{10}Be^{2+}$ per anode was according to the measurements. This resulted in a pressure of 13.5 mbar for the simulations, which agrees with the 13 mbar read by the sensor during the measurement.
With these parameters the position of the measured $^{10}Be^{2+}$ is well matched to the outcome of the simulations. The red dot in Fig. 4.3 displays the output of the simulated position of the $^{10}Be^{2+}$ peak. Expecting to detect parts of broken up molecules, especially with a $m/q$-ratio of 5, and some other ions, several particles were simulated. A list of the simulated particles and their initial energies can be found in Tab. 4.1 and their origins are described in the sections 4.2.1.1 to 4.2.1.3.

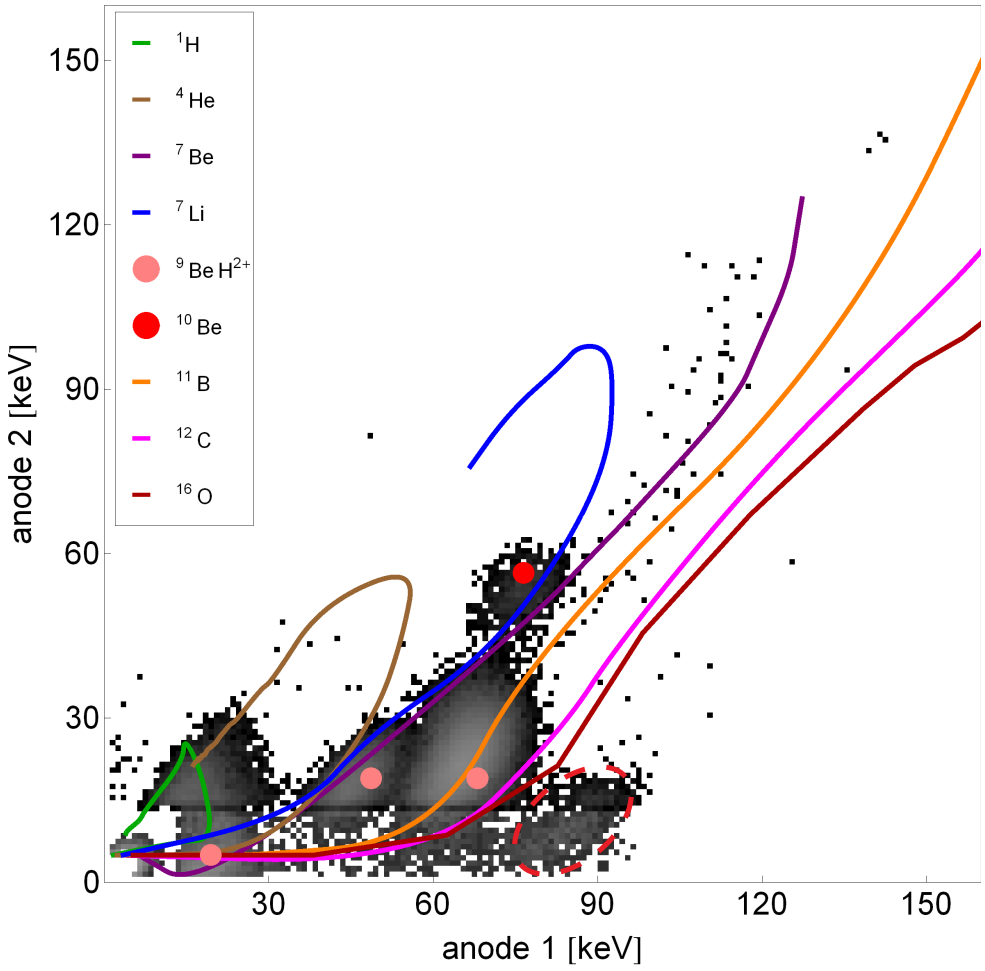


**Figure 4.3.:** The measured spectrum shown in gray in this figure is an overlay of measured energy-loss spectra from three sample materials: Beryllium-Oxide, ATI-Be standard and a Phenakite blank. The colored dots and lines show the results of the simulations with SRIM. The simulations were done to identify the background of the measurements. The red dot indicates the location of the simulated $^{10}Be^{2+}$ and the pink dots indicate the simulations of the molecule $^{9}Be^{1}H^{2+}$ . The peak marked by the dotted red circle has not been identified through the simulations, it is expected to be either $^{16}O$ or $^{12}C$. $^{7}Li$ would cause a real background in the area of the $^{10}Be^{2+}$ peak but the absence of events along the simulated $^{7}Li$-tail indicates that it is not present in the beam.

#### 4.2.1.1. Products of nuclear reactions

Nuclear reactions from ions hitting the SiN-foils can cause background. Reaction products of the two expected nuclear reactions

- p($^{10}$B, $\alpha$)$^{7}$Be
- p($^{15}$N, $\alpha$)$^{12}$C

could be possibly detected. The first reaction comes from $^{10}B^{2+}$ ions with a maximum energy of 7.21 MeV hitting $^{1}$H inside a SiN-foil. If this leads to a forward scattering of the reaction products either $^{7}$Be or the $\alpha$ will reach their maximum energy. Those energies were derived in a non relativistic approach[3]. The maximum energy of $^{7}$Be scattered forward would be 8.13 MeV and the $\alpha$ particle in a forward direction would have an energy of 6.83 MeV.

The second reaction is the result of a $^{15}N^{3+}$ ion hitting $^{1}$H in the SiN-foils. The maximum nominal energy would be 10.81 MeV. Due to the same $m/q$ as $^{10}B^{2+}$ and $^{10}Be^{2+}$ it is possible for the ion to pass through the mass spectrometer. When it hits a $^{1}$H the reaction products are $^{12}$C which receives an energy of 15.56 MeV when it is forward scattered and an $\alpha$ particle with a maximum energy of 13.32 MeV in forward direction.

#### 4.2.1.2. Molecules

As mentioned before, all ions with the same $m/q$-ratio can pass through the mass spectrometer and can possibly be detected in the background. For the measurements of $^{10}Be^{2+}$ the mass spectrometer was set to $m/q = -26$ on the low energy side while $m/q = 5$ was selected on the high energy side. Therefore these are possible ions that might appear in the background:

- $^{9}Be^{1}H^{2+}$ from the molecule $^{9}Be^{16}O^{1}H^{-}$
- $^{15}N^{3+}$ from the molecule $^{15}N^{9}Be^{1}H_{2}^{-}$
- $^{25}Mg^{5+}$ from the molecule $^{25}Mg^{1}H^{-}$

[3]Compared to the relativistic results from [Catford, W. (2004)] the differences can be neglected

In the simulations 53 % of $^{25}Mg^{5+}$ and 24 % of $^{15}N^{3+}$ pass through the foils. They appear in the lower left edge of Fig. 4.3 because they have such a low energy ($^{25}Mg^{5+}$ with a maximum energy of 116 keV and $^{15}N^{3+}$ with an energy $< 25$ keV) that they are stopped on the first anode right after entering the detector. The molecule $^{9}Be^{1}H^{2+}$ is broken up when it hits the first foil and the total energy is distributed among the two fragments. 9/10 of the energy goes to $^{9}Be$ and 1/10 of the energy is transmitted to $^{1}H$. This causes three different peaks in the spectrum (pink dots in Fig. 4.3) because either one or both of the two parts of the molecule can enter the detector. $^{1}H$ with a maximum energy of 0.72 MeV generates the pink dot on the left and $^{9}Be$ with a maximum energy of 6.48 MeV generates the pink dot in the middle. If both particles enter the ionization chamber at the same time they are detected together and their signals are summed up generating the pink dot on the right.

#### 4.2.1.3. Others

In Tab. 4.1 there are ions listed that have not yet been discussed. Simulations were made for all elements up to the mass 16 to find out if they can be excluded from the background. $^{7}Li$ can produce a harmful background in the $^{10}Be$ bin but is not observed in measurements. It has the wrong $m/q$-ratio and is not able to produce a matching molecule. There is an unidentified peak circled in red, which shows up in blank measurements with a long recording time. This could be $^{16}O$ or $^{12}C$.

## 4.3. Environmental samples

### 4.3.1. Remeasurement of known samples

To confirm the reliability of the new developed foil stack method, known samples were remeasured and compared to the results of past measurements with the gas absorber as well as the degrader foil method. The samples underwent different chemical preparations and were used to exclude unexpected background from other ions in measurements of environmental samples.

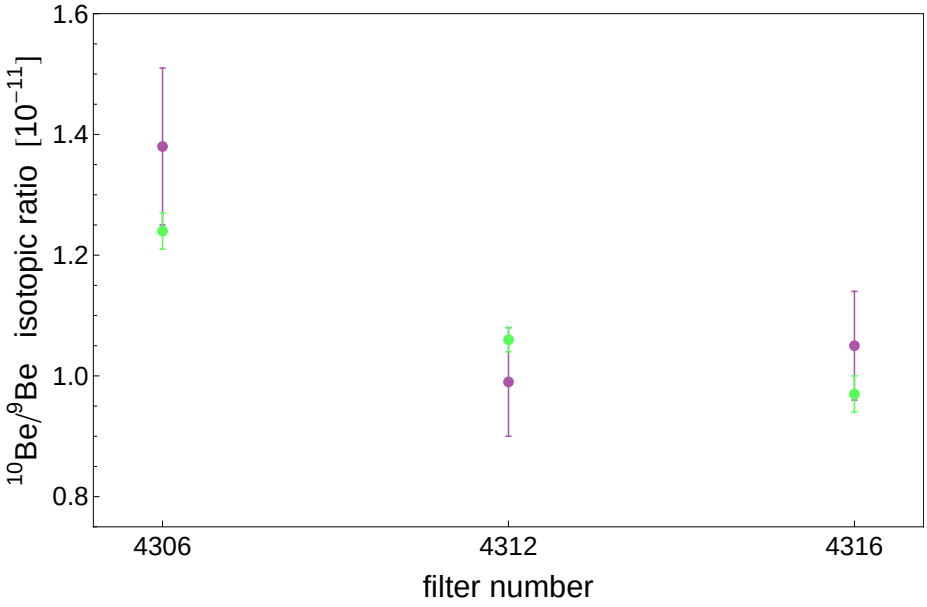


**Figure 4.4.:** Shown in this figure are normalized isotopic ratios of samples from the STACCATO-project recorded with the gas absorber method (purple) and ratios re-measured with the foil stack method (green). The error bars are given by statistical uncertainties. It can be seen that there is no systematic offset between those datasets.

#### 4.3.1.1. Atmospheric particle-bound $^{10}$Be samples

In the framework of the EU project STACCATO[4], [Priller et al. (2004)] investigated the connection between the atmospheric transport processes and the $^{10}$Be/$^{7}$Be ratio. For this purpose, particle-bound beryllium isotopes were collected at three meteorological stations: Sonnblick (Austria), Zugspitze (Germany) and Jungfraujoch (Switzerland). While $^{7}$Be was measured using its characteristic gamma-radiation the $^{10}$Be measurement at VERA was done with the gas absorber method.

Three filter samples were taken from the set of the STACCATO-project and measured with the foil stack method. Results from both methods were normalized to the S555 standard. In 2004 a beryllium half-life of $t_{1/2} = 1.51$ Ma [Hofmann et al. (1987)] was used. For comparison the data from 2004 were corrected with the updated half-life of $t_{1/2}$=1.39 Ma

Fig. 4.4 shows the results of both methods. In green are the results of the foil stack

[4]Influence of Stratosphere-Troposphere Exchange in A Changing Climate on Atmospheric Transport and Oxidation Capacity

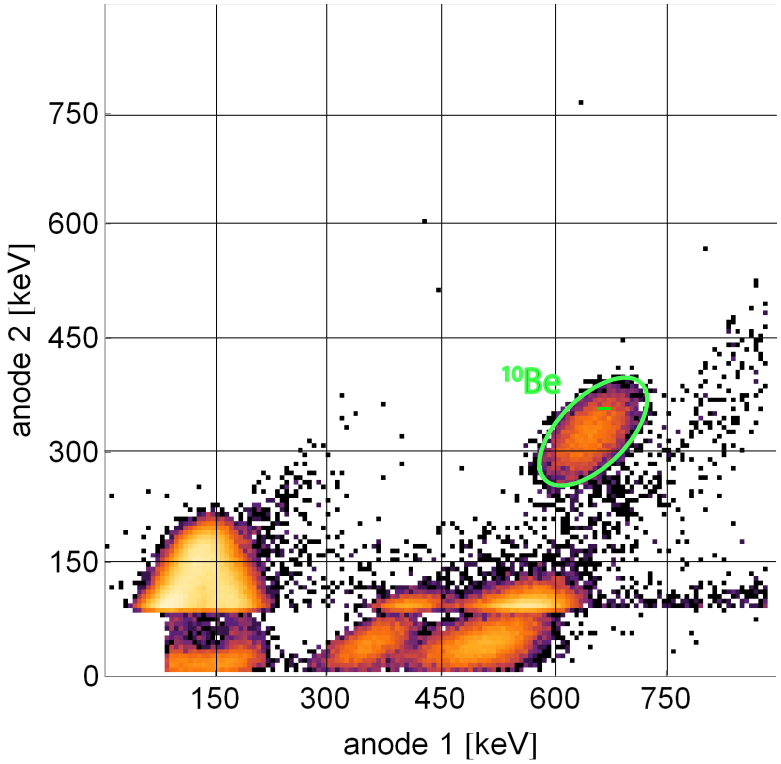


**Figure 4.5.:** This figure shows a two-dimensional energy-loss spectrum of filter 4306 of the STACCATO-project (see Fig 4.4) with an acquisition time of $\sim 60\,min$. Even though the background causes a very high count rate, this two-dimensional spectrum does not show any peaks that could not be identified by the simulations (see sections 4.2).

method measured during this thesis. The purple data points show the outcome with the gas absorber method in 2004. The comparison shows that the data agree very well within their uncertainties. Although the background has a very high count rate, no unexpected peaks are detected that could cause disturbance in the $^{10}$Be bin. The background from the randomly elected filter 4306 can be seen in the two-dimensional energy-loss spectrum Fig. 4.5.

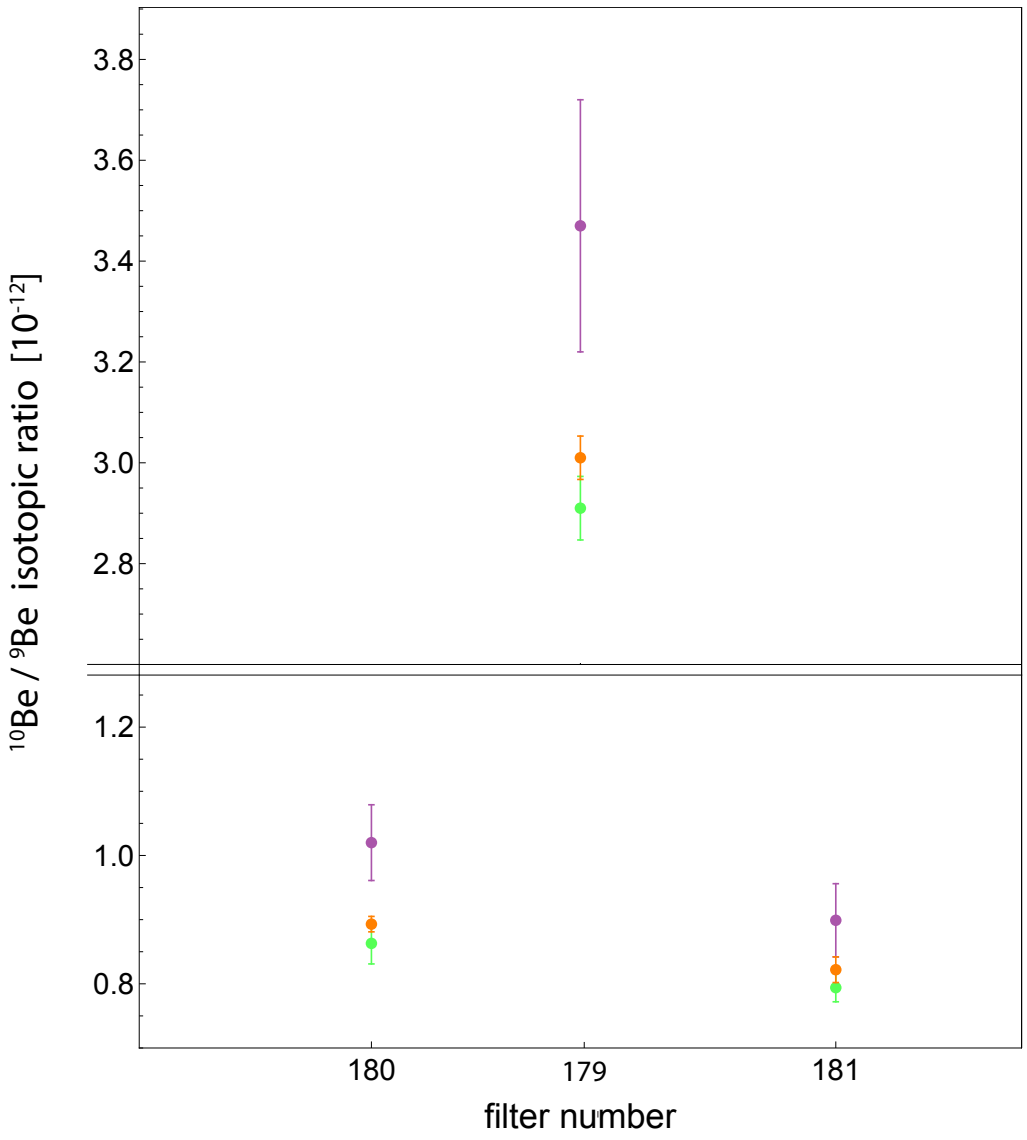


**Figure 4.6.:** These figures show $^{10}$Be/$^{9}$Be ratios of ice core samples. In purple are the data recorded at VERA with the degrader foil method and normalized to the SRM 4325 standard. The results of the measurements with the foil stack method are plotted in green. Due to an offset in the measurement the data differ by 12 %. In orange are the results of the foil stack method corrected by a 4 % difference between the measured ATI-Be standard value and its nominal value.

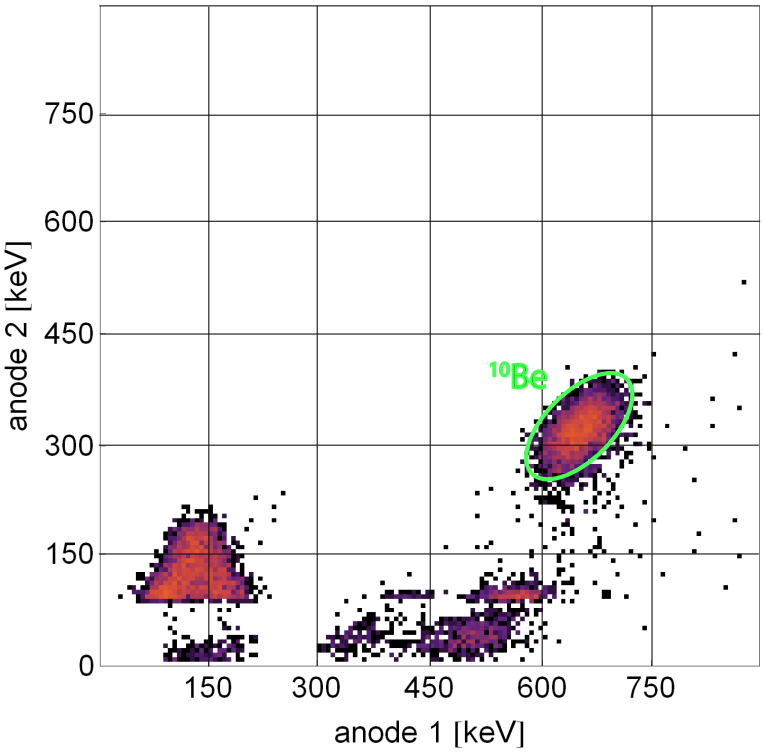


**Figure 4.7.:** This figure shows the two-dimensional energy-loss spectrum of ice core sample 179 with an acquisition time of $\sim 15\,min$. $^{10}$Be can be well separated from the background that does not show any unexpected peaks.

#### 4.3.1.2. $^{10}$Be ice core samples

To compare the foil stack method with the degrader foil method at the VERA facility three samples were taken from a project aiming at radiometric dating of ancient ice via the $^{26}$Al/$^{10}$Be ratio done in [Auer et al. (2009)].
The comparison of results can be seen in Fig. 4.6. The results measured with the degrader foil method were normalized to the SRM 4325[5] standard in 2012 and are marked purple. Green are the results of the foil stack method. These measurements show an offset of 12 %. A possible explanation would be that the Standard, ATI-Be, which was measured along for normalization, is inhomogeneous. This standard was used due to the fact that some of the simultaneously measured samples were expected to be low. To avoid cross contamination we did not use a high standard as S555. The possible inhomogeneity of ATI-Be was unknown to us until

[5]The SRM 4325 standard has a nominal value of $(2.79 \pm 0.03) \times 10^{-11}$

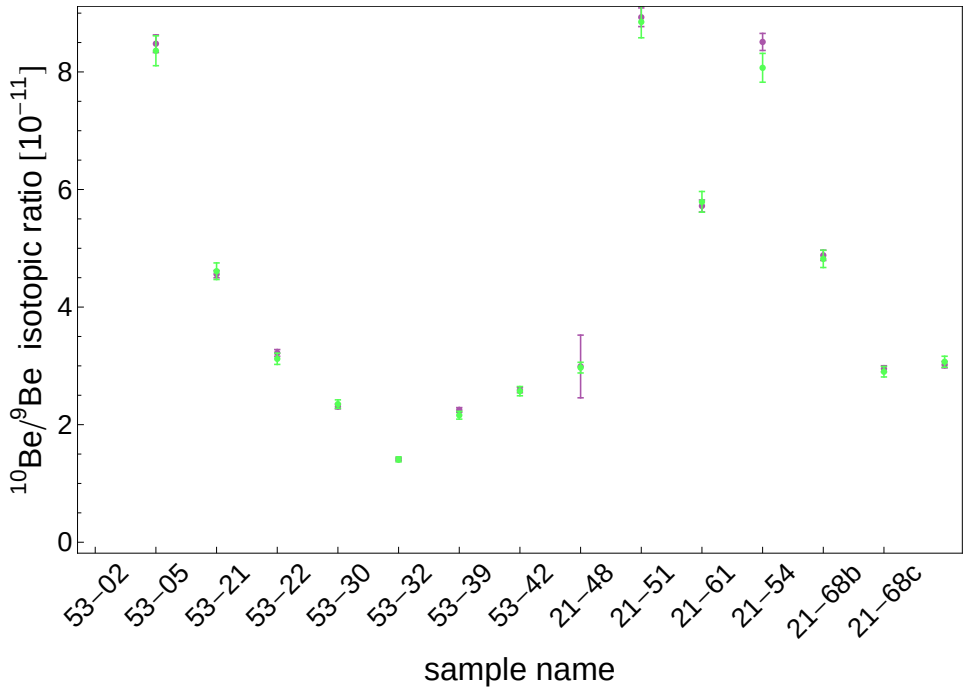


**Figure 4.8.:** Both figures show the $^{10}$Be/$^{9}$Be isotopic ratio for samples derived from a marine sediment core. In purple are the results from the DREAMS facility in Dresden where $^{10}$Be is measured with the degrader foil method, green is the outcome of the measurements with the foil stack method at the VERA facility.

the end of the measurement. However, further investigations are needed to verify this interpretation.

The normalization was corrected by 4 %, given by the offset of the measured ATI-Be ratio from its nominal $^{10}$Be/$^{9}$Be ratio. The so corrected data are plotted in orange. Unfortunately, the origin of the 12 % offset has not yet been understood. This is the only measurement that deviates, but it does not seem to be trustworthy. However, the background appearing in the measurements did not show unexpected peaks and the $^{10}$Be peak is well separated as shown in Fig. 4.7.

### 4.3.2. Measurement of samples with unknown $^{10}$Be content

For the dissertation of Mag. Jenny Feige, samples with previously unknown $^{10}$Be content were measured. In [Feige et al. (2012)] they report about possible supernova produced radionuclides in terrestrial deep-sea archives. For their analyses two suitable marine sediment cores were taken from the South Australian Basin.

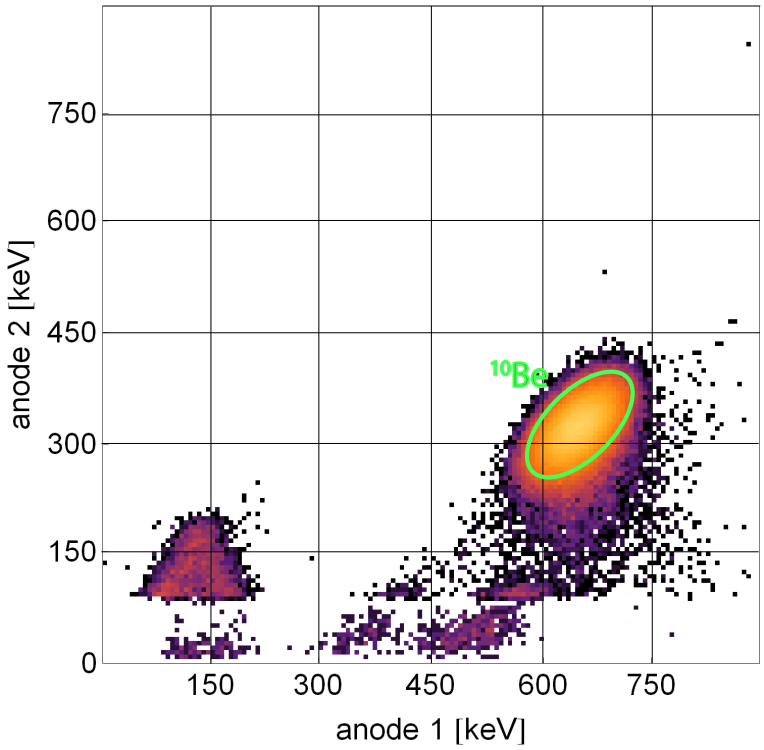


**Figure 4.9.:** This figure shows a two-dimensional energy-loss spectrum sample 21-51 with an acquisition time of $\sim 15\,min$. The count rate of $^{10}$Be is very high in comparison to the background.

To date the the layers of the sediment core $^{10}$Be is used.
In Fig. 4.8 results of the two methods are compared. The data plotted in purple were recorded at the DREAMS facility in Dresden where the degrader foil method is used [Akhmadaliev et al. (2012)].
The data are normalized to the SMD-Be-12 standard (see section 4.1.1). Results of the measurements with the foil stack method at VERA are shown in green and were normalized to the S555 standard (see section 4.1.1). The measurements agree very well with each other. The background shows low peaks caused by $^{9}Be^{1}H^{2+}$. The two-dimensional energy-loss spectrum of sample 21-51 can bee seen in Fig. 4.9.

# 5. Summary and Outlook

Using a SiN-foil stack to separate $^{10}$Be from $^{10}$B has proven to work very satisfying. The foil stack method significantly improved the measurement of $^{10}$Be and will be used in the future at VERA.
In Tab. 5.1, the performance of the foil stack method is compared to the degrader foil and the gas absorber method, used at VERA in the past. With the foil stack method it is possible to increase the negative ion detection efficiency to a very high 45 %. The reproducibility for samples with a ratio $^{10}\mathrm{Be}/^{9}\mathrm{Be} > 10^{-12}$ could be improved to 0.3 % and the background has been reduced to $^{10}\mathrm{Be}/^{9}\mathrm{Be} < 7 \times 10^{-16}$. With its good statistics and steady behavior for different environmental samples the foil stack method combines the advantages of both methods used in the past.

Despite great improvements over the old methods, several issues need to be further investigated. First of all the reasons for the general deviation of one measurement series needs to be uncovered. The areal density derived from the energy-loss of alpha particles $(2650 \pm 50)\,\mu g/\mathrm{cm}^2$ fits the nominal areal density of

| | degrader foil | gas absorber | foil stack |
|---|---|---|---|
| negative ion detection efficiency | 15 % | 5 % | 45 % |
| reproducibility for samples $^{10}\mathrm{Be}/^{9}\mathrm{Be} > 10^{-12}$ | 3 % | 1 % | 0.3 % |
| background ($^{10}\mathrm{Be}/^{9}\mathrm{Be}$) | $< 10^{-15}$ | $1 \times 10^{-14}$ | $7 \times 10^{-16}$ |

**Table 5.1.:** The comparison of the methods shows the improvements that were achieved using the foil stack method. All values are results of measurement at the VERA laboratory.

2480 $\mu g/cm^2$ expected after the first simulations. The areal density of 1900 $\mu g/cm^2$ derived from the measurements by taking $^{10}$Be as a reference point leads to discrepancies that have not been fully resolved and need further analysis. A part of these deviation can be explained by the 5 % uncertainty in the energy calibration, which could be improved. The gas pressure of isobutane in the measurements was between 13 mbar and 17 mbar. For the energy calibration the pressure was between 85 mbar and 107 mbar which may lead to extrapolation uncertainties. For further measurements an energy calibration, done with a lower pressure in the ionization chamber, is suggested.
The losses by angular straggling in the foil stack is according to the simulations only 0.4 % if a beam width of 2.4 mm FWHM is supposed. To identify the beam losses in the foil stack during measurements, the count rate of attenuated $^{9}$Be could be measured before entering the foil stack and than compared with the count rate in the ionization chamber. If necessary the angular straggling in the foil stack could then be reduced by using less but thicker foils. By measuring the areal density only the thickest foils can be chosen for the foil stack.
The harmful background that could be caused by $^{7}$Li should be excluded by measuring a $^{7}$Li target with the $^{10}$Be setup to determine the overall suppression factor.

# A. Config-file for MAIC-Sim

```
(* Config-File for MAIC-Sim-1c *)
(* ========================== *)

SimName = "File Name";
Ions =20000;

(*_____________________________________________________Ion-Properties *)
(*Ion1 = {2, He, 4.002603, 3.};*)
Ion2 = {4, Be, 10.013534, 7.209};
(*Ion3 = {5, B, 10.012937, 6.942};*)
(*Ion4 = {12, Mg, 24.98583, 18.023};*)
(*Ion5 = {7, N, 15.000108, 10.814};*)
(*Ion6 = {4, Be, 7.01692, 8.130};*)
(*Ion7 = {17, Cl, 35.968307, 25.};*)
(*Ion8 = {92, U, 238.050783, 16.};*)
(*Ion9 = {2, He, 4.003, 3.2};*)

EnergySigma = 0.000212; (* relative *)
BeamDiameter = ; (* FWHM in mm *)

(*_____________________________________________________Foil-Stack *)
Foils = 13; (* 0 = no foils *)
FoilThickness = 464; (* nm *)
FoilDesign = "q"; (* "q"=quadratic, ""=circular *)
FoilDia = 7.07; (* diagonal/diameter in mm *)
FoilDensity = 3.1; (* g/cm^3 *)
FoilInterspace = 1; (* mm *)
FoiltoWindowDistance = 3; (* mm *)
FoilPath = "Data_in\\SiN_TRIM.IN"; (* relative path *)
VacuumPath = "Data_in\\Air@1013_TRIM.IN"; (* relative path *)

(*_____________________________________________________Detector-Window *)
WindowThickness = 100; (* nm *)
WindowDesign = "q"; (* "q"=quadratic, " "=circular *)
WindowDia = 7.07; (* diagonal/diameter in mm *)
WindowPath = "Data_in\\SiN_TRIM.IN"; (* relative path *)

(*_____________________________________________________MAIC-Properties *)
GasPressure = 17; (* mbar *)
GasPath = "Data_in\\Isobutan@1013_TRIM.IN"; (* relative path *)
AnodeSplitting = {32}; (* mm *)
(* Anodes = 1; (* max. 999 *)*)
(* AnodeSplitting = Table[N[i AnodeLengthTotal/Anodes],{i,1,Anodes-1}]; (* mm *)*)
AnodeLengthTotal = 64; (* mm *)

(*_____________________________________________________Outputs *)
ExyzInc = 0; (* eV *) (* 0 = no EXYZ-File-Output *)
```

# B. Outputfile SRIM

```
============================== SRIM-2008.04 ==============================
==========================================================================
================  TRANSMIT.txt : File of Transmitted Ions  ================
=  This file tabulates the kinetics of ions or atoms leaving the target.     =
=  Column #1: S= Sputtered Atom, B= Backscattered Ion, T= Transmitted Ion.   =
=  Col.#2: Ion Number, Col.#3: Z of atom leaving, Col.#4: Atom energy (eV).  =
=  Col.#5-7: Last location:  X= Depth into target, Y,Z= Transverse axes.     =
=  Col.#8-10: Cosines of final trajectory.                                   =
= *** This data file is in the same format as TRIM.DAT (see manual for uses).=
====== TRIM Calc.= Be(7.20 MeV) ==> SiN(  1 um) ==============================
 Ion  Atom   Energy        Depth       Lateral-Position        Atom Direction
 Numb Numb    (eV)          X(A)        Y(A)       Z(A)      Cos(X)  Cos(Y) Cos(Z)
T    1  4 .6234239E+07   1000052E-02 -.1567E+02 -.9116E+01   .9999942  .0012409 -.0031690
T    2  4 .6284681E+07   1000178E-02  .2685E+02  .2509E+02   .9999246  .0081647  .0091690
T    3  4 .6260672E+07   1000119E-02 -.9244E+01  .5484E+02   .9999463 -.0022552  .0101169
T    4  4 .6246051E+07   1000000E-02 -.9419E+01 -.9188E+01   .9999759 -.0067439 -.0016370
T    5  4 .6266516E+07   1000174E-02 -.3089E+01  .4755E+01   .9999917  .0009152  .0039768
T    6  4 .6230935E+07   1000115E-02  .1273E+02 -.1004E+01   .9999969  .0017126 -.0017883
T    7  4 .6260466E+07   1000170E-02 -.2722E+02  .7494E+02   .9999496 -.0065770  .0075855
T    8  4 .6239795E+07   1000113E-02 -.1518E+03 -.1039E+03   .9994175 -.0246893 -.0235594
T    9  4 .6254959E+07   1000153E-02  .1420E+02  .4392E+02   .9999636  .0021258  .0082594
T   10  4 .6245831E+07   1000051E-02 -.8338E+02 -.5364E+02   .9998467 -.0154579 -.0082233
T   11  4 .6222067E+07   1000162E-02 -.7199E+02 -.3452E+02   .9998341 -.0157932 -.0090787
T   12  4 .6286720E+07   1000208E-02 -.1013E+02  .4168E+02   .9999542 -.0039565  .0087200
T   13  4 .6271375E+07   1000027E-02  .1793E+02 -.1760E+02   .9999991  .0003218 -.0013378
T   14  4 .6256471E+07   1000031E-02  .4366E+01  .3661E+02   .9999263  .0045581  .0112490
T   15  4 .6254934E+07   1000126E-02  .4603E+02  .1992E+02   .9999918  .0012820  .0038410
T   16  4 .6263067E+07   1000060E-02  .2134E+01  .2797E+02   .9999438  .0013450  .0105152
T   17  4 .6223338E+07   1000175E-02 -.5575E+02 -.1685E+02   .9999761 -.0062616 -.0029212
```

# Bibliography

Akhmadaliev, S., Heller, R., Hanf, D., Rugel, G., and Merchel, S. (2012). The new 6MV AMS-facility DREAMS at Dresden. *Nuclear Instruments and Methods in Physics Research Section B: Beam Interactions with Materials and Atoms*, 294:5–10.

Alimov, V., Synal, H., Finkel, R., and Wilcken, K. (2009). New Primary Be-10 Standard and T1/2 for AMS ETH Zürich - Recalibration of the ih-house Be-10 standards. *ETH Zurich Annual Report*, page 12.

Auer, M., Kutschera, W., Priller, A., Wagenbach, D., Wallner, A., and Wild, E. M. (2007). Measurement of $^{26}$Al for atmospheric and climate research and the potential of $^{26}$Al/$^{10}$Be ratios. *Nuclear Instruments and Methods in Physics Research Section B: Beam Interactions with Materials and Atoms*, 259:595–599.

Auer, M., Wagenbach, D., Wild, E. M., Wallner, A., Priller, A., Miller, H., Schlosser, C., and Kutschera, W. (2009). Cosmogenic 26Al in the atmosphere and the prospect of a 26Al/10Be chronometer to date old ice. *Earth and Planetary Science Letters*, 287:453 – 462.

Buchriegler, J. (2013). Construction of a Multi-Anode Ionization Chamber for AMS at VERA. Master's thesis, University of Vienna.

Catford, W. (2004). *Catkin2.02*. http://personal.ph.surrey.ac.uk/ phs1wc.

Christl, M., Lippold, J., Steinhilber, F., Bernsdorff, F., and Mangini, A. (2010). Reconstruction of global $^{10}$Be production over the past 250 ka from highly accumulating Atlantic drift sediments. *Quaternary Science Reviews*, 29:2663–2672.

Döbeli, M., Kottler, C., Stocker, M., Weinmann, S., Synal, H.-A., Grajcar, M., and Suter, M. (2004). Gas ionization chambers with silicon nitride windows for

the detection and identification of low energy ions. *Nuclear Instruments and Methods in Physics Research Section B: Beam Interactions with Materials and Atoms*, 219:415–419.

Feige, J., Wallner, A., Winkler, S. R., Merchel, S., Fifield, L. K., Korschinek, G., Rugel, G., and Breitschwerdt, D. (2012). The Search for Supernova-Produced Radionuclides in Terrestrial Deep-Sea Archives. *Astrophysics*, 29:109–114.

Forstner, O., Michlmayr, L., Auer, M., Golser, R., Kutschera, W., Priller, A., Steier, P., and Wallner, A. (2008). Applications of a compact ionization chamber in AMS at energies below 1 MeV/amu. *Nuclear Instruments and Methods in Physics Research Section B: Beam Interactions with Materials and Atoms*, 266:2213–2216.

Gosse, J. (2001). Terrestrial in situ cosmogenic nuclides: theory and application. *Quaternary Science Reviews*, 20:1475–1560.

Hofmann, H., Beer, J., Bonani, G., Gunten, H. V., Raman, S., Suter, M., Walker, R., Walfli, W., and Zimmermann, D. (1987). 10Be: Half-life and AMS-standards. *Nuclear Instruments and Methods in Physics Research Section B: Beam Interactions with Materials and Atoms*, 29:32 – 36.

Korschinek, G., Bergmaier, A., Faestermann, T., Gerstmann, U., Knie, K., Rugel, G., Wallner, A., Dillmann, I., Dollinger, G., von Gostomski, C. L., Kossert, K., Maiti, M., Poutivtsev, M., and Remmert, A. (2010). A new value for the half-life of 10Be by Heavy-Ion Elastic Recoil Detection and liquid scintillation counting. *Nuclear Instruments and Methods in Physics Research Section B: Beam Interactions with Materials and Atoms*, 268(2):187 – 191.

Kutschera, W. (1990). Accelerator mass spectrometry: A versatile tool for research. *Nuclear Instruments and Methods in Physics Research Section B: Beam Interactions with Materials and Atoms*, 50:252 – 261.

Kutschera, W., Collon, P., Friedmann, H., Golser, R., Hille, P., Priller, A., Rom, W., Steier, P., Tagesen, S., Wallner, A., Wild, E., and Winkler, G. (1997). VERA: A new AMS facility in Vienna. *Nuclear Instruments and Methods*

*in Physics Research Section B: Beam Interactions with Materials and Atoms*, 123:47 – 50.

Lal, D. (1991). Cosmic ray labeling of erosion surfaces: in situ nuclide production rates and erosion models. *Earth and Planetary Science Letters*, 104:424 – 439.

Lal, D., P. B. (1967). *Cosmic - Ray Produced Radioactivity on the Earth.* Pordue University.

Martschini, M. (2008). 10Be - 10B isobar separation with a degrader foil: Implementation and testing of an optimized ion -optical setup for AMS of 10Be. Master's thesis, University of Vienna.

Merchel, S., Arnold, M., Aumaître, G., Benedetti, L., Bourlès, D., Braucher, R., Alfimov, V., Freeman, S., Steier, P., and Wallner, A. (2008). Towards more precise 10Be and 36Cl data from measurements at the 10-14 level: influence of sample preparation. *Nuclear Instruments and Methods in Physics Research Section B: Beam Interactions with Materials and Atoms*, 266(22):4921–4926.

Michlmayer, L. (2007). Isobar separation wih post-stripping for the measurement of cosmogenic 10Be at VERA. Master's thesis, University of Vienna.

Middleton, R. (1990). *Negative-Ion Cookbook.* Department Of Physics, University of Pennsiylvenia.

Priller, A., Berger, M., Gäggeler, H. W., Gerasopoulos, E., Kubik, P. W., Schnabel, C., Tobler, L., Wild, E.-M., Zanis, P., and Zerefos, C. (2004). Accelerator mass spectrometry of particle-bound 10Be. *Nuclear Instruments and Methods in Physics Research Section B: Beam Interactions with Materials and Atoms*, 223-224:601 – 607.

Priller, A., Brandl, T., Golser, R., Kutschera, W., Puchegger, S., Rom, W., Steier, P., Vockenhuber, C., Wallner, A., and Wild, E. (2000). Extension of the measuring capabilities at VERA. *Nuclear Instruments and Methods in Physics Research Section B: Beam Interactions with Materials and Atoms*, 172:100–106.

Sheng Xu, Dougans, A. B., Freeman, S. P., Schnabel, C., and Wilcken, K. M. (2010). Improved 10Be and 26Al - AMS with a 5MV spectrometer. *Nuclear*

*Instruments and Methods in Physics Research Section B: Beam Interactions with Materials and Atoms*, 268:736 – 738.

Silson Ltd (2012). *Silson Ltd, JBJ Business Park, Northampton Road, Blisworth, Northampton, NN7 3DW, England,*. Silson Ltd.

Stanford Research (1980). *Stanford Research System, Synnvale, California USA*. Stanford Research.

Steier, P., Golser, R., Liechtenstein, V., Kutschera, W., Priller, A., Vockenhuber, C., and Wallner, A. (2005). Opportunities and limits of AMS with 3-MV tandem accelerators. *Nuclear Instruments and Methods in Physics Research Section B: Beam Interactions with Materials and Atoms*, 240:445 – 451.

Steier, P., Puchegger, S., Golser, R., Kutschera, W., Priller, A., Rom, W., Wallner, A., and Wild, E. (2000). Developments towards a fully automated AMS system. *Nuclear Instruments and Methods in Physics Research Section B: Beam Interactions with Materials and Atoms*, 161-163:250 – 254.

Vockenhuber, C., Ahmad, I., Golser, R., Kutschera, W., Liechtenstein, V., Priller, A., Steier, P., and Winkler, S. (2003). Accelerator mass spectrometry of heavy long-lived radionuclides. *International Journal of Mass Spectrometry*, 223 - 224:713 – 732.

Wallner, A., Coquard, L., Dillmann, I., Forstner, O., Golser, R., Heil, M., Käppeler, F., Kutschera, W., Mengoni, A., Michlmayr, L., Priller, A., Steier, P., and Wiescher, M. (2008). Measurement of the stellar cross sections for the reactions $^{9}$Be(n,$\gamma$)$^{10}$Be and $^{13}$C(n,$\gamma$)$^{14}$C via AMS. *Journal of Physics G Nuclear Physics*, 35:014018.

Ziegler J.F., Biersack J.P., Ziegler M.D. (2008). *SRIM The Stopping and Range of Ions in Matter*.

# Acknowledgments

First, I want to thank Robin Golser for giving me the opportunity to do my diploma thesis at the VERA facility. I am grateful to Peter Steier and Alfred Priller for their support and advice during this time. Further I want to thank Toni Wallner, Silke Merchel, Jenny Feige, Eva Maria Wild and Alfred Priller for giving me the possibility to measure or remeasure samples from their projects and take their data for comparison. Special thanks to Martin Martschini who invested a lot of his time proofreading my thesis. Also I want to thank my colleagues Jenny, Josef and Thomas for making the breaks so entertaining and even informative sometimes. And last, thanks to the whole VERA staff especially the workshop who was always ready to help.

Besonderer Dank geht an Josef Papauschek, für alles. Auch meiner Studienkollegin Mag. Josefa Großschedl möchte ich für die gegenseitige Motivation und die Wegbegleitung durch die schwere Zeit besonders danken. Danke auch an alle Beiträge zur Diplomarbeit von Markus, Mariana, Martin P. und Josef.

# Curriculum vitae

| | |
|---|---|
| Name: | **Edith Schmidt** |
| Place of birth: | Vienna, Austria |
| Nationality: | Austria |

## Education

| | |
|---|---|
| 1986 – 1990: | Elementary school , 1060 Vienna, Austria |
| 1990 – 1995: | Secondary school, 1070 Vienna, Austria |
| 1995 – 1996: | Vienna Business School, 1080 Vienna, Austria |
| 2004 – 2006: | Eligibility for studying at the University of Vienna |
| 2004 – 2007: | Bachelor Study of Astronomy at the University of Vienna |
| since Sept. 2007 | Master Study of Astronomy at the University of Vienna |
| | Master Study of Physics at the University of Vienna |
| since April 2011 | Diploma thesis at the VERA Laboratory, Faculty of Physics |
| | University of Vienna (supervisor: Prof. Robin Golser): |
| | *"AMS detection of $^{10}$Be with a SiN-foil stack"* |

## Working Experience

| | |
|---|---|
| 1995 – 2007: | Office work at Chartered accountant |
| | Mag. Eva Schmidt |
| Winter 2001/2002 | Skiing Instructor |
| 2002 – 2003: | Barista |
| | Austrian Star Gastronomie GMBH |
| since 2006: | Cash desk and sale |
| | Zeiss Planetarium and Urania observatory Vienna |
| Winter 2006/2007: | Tutor for the exercise of "Introduction to Astronomy" |
| 2007 – 2009: | Student government astronomy |

## Publications

A. Pigulski, G.Handler, G.Michalska, Z.Kolaczkowski, G.Kopacki, A.Narwid, E.Vanhollebeke, M.Steslicki, K. Lefever, K.Gazeas, W.DeMeester, J. Vanautgaerden, A. Leitner, J.De Ridder, V. Van Helshoecht, C. Gielen, B. Vandenbussche, S.Saesen, M.D.Reed, J.R. Eggen, G.A. Gelven, M.Desmet, E.Puga Antolin, C.Aerts, E.Schmidt, R. Huygen, D.Lorenz, M.Vuckovic, E.Broeders, E.Bauwens, T.Verhoelst, P.Deroo, P.Lenz, S.Dehaes, D. Ladjal, B. Steininger, G.Davignon, P. Beck, K.Yakut, R.Drummond, J.N.Fu7, X.J. Jiang, C. Zhang, J. Provencal, L.Decin, *The ongoing 2005 – 2006 campaign on $\beta$ Cephei stars in NGC 6910 and $\chi$ Persei (NGC 884)*, Communication in Asteroseismology 148 (2006)

## Conference contributions

Annual ÖPG Meeting, 18 – 21 Sept. 2012, Graz, Austria
*"AMS detection of Be-10 with a silicon nitride foil stack: higher efficiency, lower background"*, presented as talk